OE Optical Engineering

REVIEW

Optical fiber sensors for water and air quality monitoring: a review

Dajuan Lyu,[a,b] Qing Huang,[c,*] Xiaokun Wu,[d] Yanbo Nie,[a,b] and Minghong Yang[a,*]
[a]Wuhan University of Technology, National Engineering Research Center for Fiber Optic Sensing Technology and Networks, Wuhan, China
[b]Yangtze Optical Fibre and Cable Joint Stock Limited Company, State Key Laboratory of Optical Fiber and Cable Manufacture Technology, Wuhan, China
[c]Huazhong University of Science and Technology, School of Integrated Circuits, Wuhan National Laboratory for Optoelectronics, Optics Valley Laboratory, Wuhan, China
[d]Wuchang Shipbuilding Heavy Industry Group Co., Ltd., Wuhan, China

ABSTRACT. Owing to their advantages of anti-electromagnetic interference, chemical resistance, high sensitivity, and fast response time, optical fiber sensors (OFSs) are widely used in biomedical, environmental monitoring, and food safety fields. We introduce the classification and principles of OFSs and summarize the applications and research progress of OFSs in water quality detection (heavy metals and microorganisms) and air quality monitoring (CO*x*, NO*x*, and VOCs). Meanwhile, analytical performance, reliability, and environmental adaptability of OFSs are discussed and prospected.

 [DOI: 10.1117/1.OE.63.3.031004]

Keywords: optical fiber; environmental monitoring; gas sensor; heavy metals; volatile organic compounds

Paper 20230783SSV received Aug. 28, 2023; revised Oct. 20, 2023; accepted Oct. 24, 2023; published Nov. 8, 2023.

1 Introduction

Optical fiber-sensing technology enables the monitoring of physical, chemical, biological, and other parameters by utilizing the propagation properties of light in optical fibers.[1,2] The fiber sensor comprises a light source, incident and outgoing fibers, an optical modulator, an optical detector, and a demodulator. The principle of optical fiber-sensing technology is based on the transmission and modulation of light. Light from the light source is transmitted through the incident fiber to the modulator, where the parameters to be measured interact with the light entering the modulation zone, resulting in changes in the optical properties of the light (such as intensity, wavelength, frequency, phase, and polarization). The modulated light is then transmitted through the outgoing fiber to the photodetector and demodulator to obtain the measured parameters. Optical fiber-sensing technology offers high sensitivity, accuracy, corrosion resistance, long-distance measurement, anti-electromagnetic interference, and other advantages. It is widely used in fields such as chemical industry, aviation, aerospace, earthquake, medical treatment, and environmental health.[3–8]

Environmental health mainly involves monitoring and evaluating pollutants and harmful substances, which is an essential aspect of environmental protection and public health. It plays a vital role in ensuring public health, promoting sustainable development, protecting the environmental ecosystem, and advancing scientific and technological innovation. Conventional methods, such as ultraviolet and visible (UV–vis) spectrophotometry,[9] infrared spectroscopy,[10,11] and nuclear magnetic resonance[12,13] for environmental health assessment, are frequently

*Address all correspondence to Qing Huang, qinghuang@hust.edu.cn; Minghong Yang, minghong.yang@whut.edu.cn

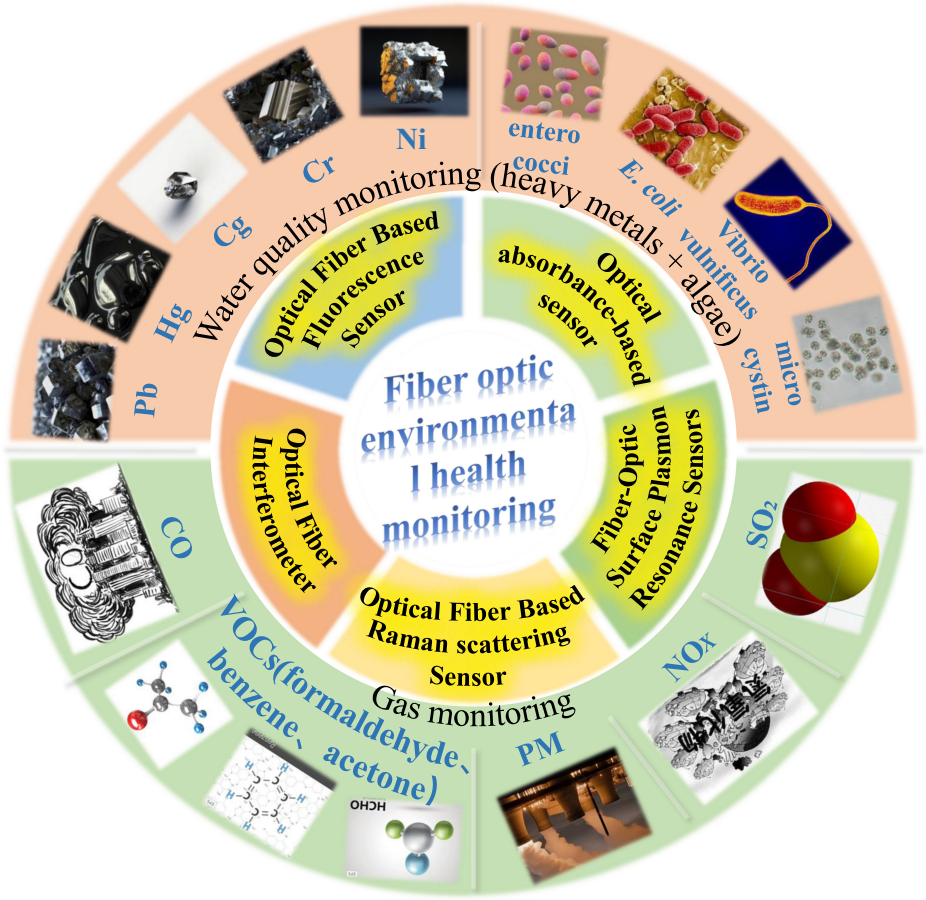

Fig. 1 Overview of optical fiber-sensing technology in the environmental health monitoring.

characterized by their time-consuming and labor-intensive nature, encompassing intricate procedures, such as manual sampling and laboratory analysis. In contrast, optical fiber-sensing technology enables real-time and long-distance monitoring of various environmental parameters, providing benefits in terms of speed, accuracy, and cost-effectiveness.[14,15]

Optical fiber-sensing technology has extensive applications in air quality monitoring and water quality monitoring, as shown in Fig. 1. Real-time monitoring of harmful substances, volatile organic compound (VOC),[16–18] CO_x,[19–21] NO_x,[22–24] SO_2,[25–27] etc.,[28] enables the provision of more accurate air quality information, facilitating effective measures for protection and improvement. Additionally, online monitoring of heavy metals, dissolved oxygen, pH, organic/inorganic pollutants, microorganisms, and other indicators in water is also of significant importance for ensuring water quality safety.

This review systematically presents recent advances in optical fiber-sensing technologies for environmental health detection. Section 2 describes the classification and principles of optical fiber sensors (OFSs) for environmental health detection, and Sec. 3 reviews the applications and research progress of OFSs in water quality detection and air quality monitoring. Section 4 summarizes the advantages and challenges of optical fiber-sensing technology in environmental health detection.

2 Classification and Basic Principles of Optical Fiber Sensor

There are various methods to classify OFSs based on the different sensing structures and principles of optical fiber. These classifications include optical absorbance-based sensor,[29,30] surface plasmon resonance (SPR) sensor,[31–33] Raman sensor,[34–36] fluorescence sensor,[37–39] and optical interference sensor.[40–42] In the following sections, we will primarily focus on an introduction to these five different types of OFSs.

2.1 Optical Absorbance-Based Sensor

Absorption spectroscopy optical fiber sensing is a technique used to gather information about a target substance by measuring the degree to which the substance absorbs light at a specific wavelength. This sensing principle is commonly used in chemical, biological, and environmental fields to detect and analyze the presence of chemicals or other specific targets in a sample.[5,43,44] As light of a specific wavelength travels through a sample, molecules or atoms in the sample may absorb the light energy. The absorbed photons excite the electrons of the molecules or atoms, causing them to jump to a higher energy level. The number of photons absorbed is proportional to the concentration of the target substance. The extent to which a sample absorbs light of a specific wavelength can be calculated by measuring the intensity of light coming back from the sample and the initial intensity of light emitted by the light source. This degree of absorption is usually represented by a plot of spectral intensity versus wavelength, known as an absorption spectrum. Based on the absorption spectrum, the properties of the target substance, such as concentration, composition, and other physical properties, can be analyzed. By comparing it with a pre-established standard spectrum, the target substance can be analyzed qualitatively. The fundamental principle of optical fiber absorption spectroscopy is illustrated in Fig. 2(a).[45] Pd nanoparticles (Pd NPs) were coated on tapered optical fibers, and when exposed to H_2 gas, H_2 molecules migrate toward the Pd-coated surface, where they interact with Pd atoms. The potential energy of these gas molecules reaches a minimum at approximately one molecular radius, causing the adsorption of H_2 gas in the conical region of the fiber. Subsequently, the adsorbed gas molecules undergo dissociation into hydrogen atoms, which then diffused within the metal structure, and culminating in the observed hydrogen absorption by the Pd structure.

2.2 Surface Plasmon Resonance Sensor

SPR optical fiber sensing is a highly sensitive and real-time biochemical sensing technique. The fundamental principle of SPR optical fiber sensing is based on the coupling phenomenon between light at the metal–medium interface and the freely moving electrons (plasma) on the metal surface.[49,50] Adjusting the angle of light incidence enables observation of changes in the reflected light's intensity. When the angle of incidence aligns with the plasma resonance angle of the metal surface, a pronounced alteration in the reflected light occurs, and this angle is known as the resonance angle. Upon the specific binding of a target molecule (e.g., protein, DNA, or chemical molecule) within the sample to a biomolecule (e.g., an antibody, oligonucleotide, or affinity ligand) immobilized on the metal film, the refractive index (RI) of the sample surface

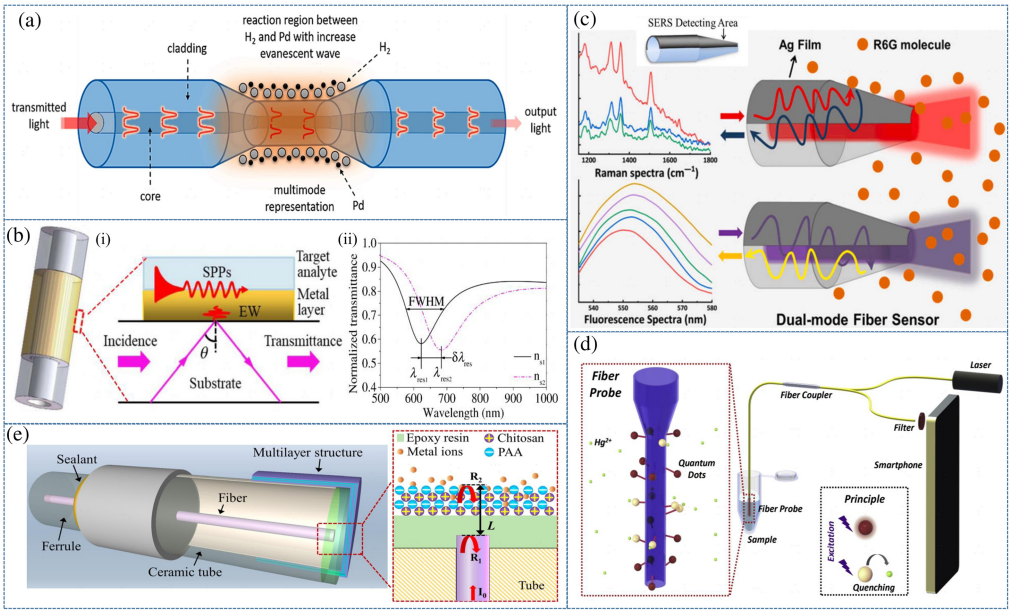

Fig. 2 Optical fiber-sensing principle: (a) optical absorbance-based sensor,[45] (b) SPR sensor,[31] (c) Raman sensor,[46] (d) fluorescence sensor,[47] and (e) optical fiber interferometric sensor.[48]

alters.[51–53] This, in turn, affects the conditions governing light propagation across the metal–medium interface, leading to a shift in the resonance angle. As shown in Fig. 2(b),[31] the decomposition of the cylindrical surface in the fiber offers an explanation for SPR phenomenon at each point, outlining a three-layer structure comprising the substrate layer, the intrinsic layer, and the dielectric layer. The substrate may consist of commercial fiber types [such as multimode fiber (MMF), photonic crystal fiber (PCF), and hollow fiber], custom fiber (such as suspended core fiber), fiber Bragg grating (FBG), etc. The intrinsic layer is composed of single or bimetallic films (such as Au, Ag, Cu, and Al) with high reflectivity and low absorptivity.[54,55] The medium layer refers to the analyte layer. It leverages the interaction of light with surface plasma at the metal–medium interface to monitor various processes on the sample surface, including molecular interactions, adsorption, and desorption. This technology finds extensive applications in biosensing, medical diagnostics, and food testing.

2.3 Raman Sensor

Raman spectroscopy, derived from molecular vibrations, offers the benefits of providing rich molecular information and being impervious to water environment, earning it the moniker "fingerprint spectrum."[56,57] A laser light source is guided to the sample through the fiber, capturing the scattered light signal and yielding the Raman scattering spectrum, replete with valuable chemical insights encompassing the sample's chemical composition, molecular structure and functional group. Comparing these spectra to reference standards stored in the database enables the effective identification and quantification of chemical substances within the target sample.

Furthermore, the intensity of the Raman scattering spectrum correlates directly with the concentration of the target molecule in the sample, facilitating precise quantitative analysis of the target compound, thereby enabling the accurate analysis and detection of samples. Optical fiber Raman scattering sensors have extensive applications in chemical analysis, biomedicine, environmental monitoring, and other domains.

Combined with the powerful enhancement effect of nanostructured metals, it becomes feasible to create a surface-enhanced Raman scattering (SERS) sensor that is both highly specific and sensitive, allowing for the non-contact, real-time collection of chemical data in samples.[58–60] As shown in Fig. 2(c),[46] the dual-mode fiber sensor was crafted through a two steps: involving tapering and half-coating. In this design, only half of the fiber tip's surface is coated with Ag film, enabling the enhancement and detection of Raman signal on the coated half surface. SERS predominantly operates as a near-field phenomenon, finely attuned to factors, such as intermolecular distances, hot spot geometry, and the efficacy of nanostructure coupling.[61] Consequently, enhancements in signal intensity can vary significantly across multiple orders of magnitude.

2.4 Fluorescence Sensor

Optical fiber fluorescence sensing is an advanced technology that harnesses the fluorescence phenomenon for sensing purposes. It involves introducing a fluorescent probe or substance into an optical fiber to detect the presence of a target molecule and gather valuable information such as its concentration and pH value.[62,63] This versatile sensing technology finds extensive applications in biomedicine, environmental monitoring, food safety, and other fields. Typically, an OFS comprises an optical fiber, where one end is connected to a light source to excite the fluorescent substance, and the other end is linked to a fluorescence detector to measure the intensity of the fluorescence signal. Tariq et al.[62] innovated an optode for pH measurement in alkaline environments, utilizing a pH-sensitive molecular fluorescent probe. This fluorescent molecular probe, Naphth-AlkyneOMe, is encapsulated within a cross-linked polyvinyl alcohol-glutaraldehyde (GA) matrix, yielding thin films characterized by well-defined physicochemical and photophysical properties. These sensing films, boasting an average thickness of 150 μm, exhibit responsive and reversible behavior in the face of pH fluctuations. The optode's applicability to authentic cementitious materials has been empirically demonstrated through pH measurements conducted during the initial hydration stage of low-pH cement paste. These measurements yield precise results with an accuracy of ± 0.1 pH units and a rapid response time of $\sim$100 s. Liu et al.[47] designed a smartphone-based optical fiber fluorescence sensor (SOFFS), as shown in Fig. 2(d). This system comprises a semiconductor laser for excitation of fluorescence signals,

a fiber probe modified with quantum dots for Hg^{2+} sensing, a smartphone equipped with a filter for collecting fluorescence signals, and a fiber coupler to connect the fiber probe, laser, and smartphone. Due to the evanescent wave on the optimized combination of a tapered fiber probe's surface, SOFFS achieves an ultralow detection limit of 1 nM and a broad detection range spanning from 1 to 1000 nM. SOFFS requires only 3 min for a single Hg^{2+} detection procedure, encompassing fiber probe replacement, recording fluorescence images, and conducting data analysis.

2.5 Interferometric Sensor

Optical fiber interferometric sensors are a cutting-edge sensing technology based on the principle of light interference. They offer numerous advantages, including high sensitivity, real-time, and remote transmission capabilities and find extensive applications in various fields, such as industry, aerospace, medical, and environmental monitoring.[64,65] The sensing fiber interacts with the physical quantity to be measured, and the reference fiber remains unaffected by the said physical quantity. When light passes through the sensing region of the optical fiber, the light waves in the sensing fiber combine with those in the reference fiber. If the sensing fiber experiences a change in its optical range due to a physical quantity, such as altering the fiber's length or RI, it leads to a modification in the phase difference between the light waves in the sensing fiber and the reference fiber. Subsequently, the combined beam of the sensing fiber and the reference fiber is directed into an interferometer, which precisely measures the phase difference between them. This alteration in phase difference is directly related to fluctuations in the optical path length within the sensing fiber, and this, in turn, corresponds to the measured physical quantity, such as pressure, temperature, or displacement. By analyzing the interference signal's variation, the value of the physical quantity can be accurately calculated. Optical demodulation is commonly employed to extract information from the interference signal and convert it into the corresponding physical quantity value.

As shown in Fig. 2(e), Yan et al.[48] applied a multilayer film comprising epoxy resin (ER), multilayer chitosan (CS), and polyacrylic acid (PAA) onto a ceramic tube. This process was undertaken to fabricate an optical fiber Fabry–Perot (F–P) sensor designed for the detection of diverse metal ions. The conventional optical fiber interferometric sensor is constructed by inserting a single-mode fiber (SMF) into a ceramic tube, which is equipped with ER on the end face to reflect light, forming the F–P interferometric cavity. Additionally, a multilayer of CS and PAA is applied to the ER's surface, serving as the sensitive film. This configuration yielded sensitivities of 9.95×10^{-4} nm ppb^{-1} for Ni^{2+}, 2.31×10^{-4} nm ppb^{-1} for Zn^{2+}, and 4×10^{-4} nm ppb^{-1} for Na^{+}. Interferometric sensors are further categorized based on their principle of operation into Mach–Zehnder interferometers (MZI),[66,67] Fabry–Perot interferometers (FPI),[68,69] Michelson interferometers (MI),[70,71] and Sagnac interferometers,[72,73] each with specific applications and advantages.

3 Water Quality Monitoring

Water plays a vital role in nature, and pollution of water significantly impacts the balance of aquatic ecosystems, causing harm to organisms and vegetation within the water. Water quality monitoring serves as an essential tool to promptly identify water pollution issues and implement measures to safeguard the water ecosystem and maintain ecological equilibrium.

OFSs offer numerous advantages in water quality monitoring, including high sensitivity, rapid response, real-time monitoring, multiparameter measurement, and long-distance transmission capabilities. These sensors exhibit exceptional sensitivity to trace water quality parameters, enabling the detection of minute pollutant concentrations and facilitating early identification of water pollution problems.[5,74] Additionally, they demonstrate strong anti-interference capabilities, ensuring stable performance even in complex water environments, without the need for direct contact with water samples. Measurement through the transmission and reflection of light prevents any damage to the water samples, making long-term stable monitoring feasible. Furthermore, OFSs allow for remote data transmission and monitoring, making them suitable for monitoring and managing a wide range of water bodies.

3.1 Heavy Metal Ion Detection

3.1.1 *Lead*

Lead (Pb) contamination poses one of the most prevalent and widespread water quality issues. Various sources contribute to lead contamination, including industrial wastewater, lead pipes, pesticides, and contaminated soil. Accumulation of lead in water bodies adversely affects aquatic organisms, disrupting the delicate balance of the entire ecosystem.[75] The consequences of lead contamination can be severe, leading to the mortality of aquatic organisms, reproductive problems, and significant ecological impacts in water bodies. Moreover, exposure to elevated lead levels raises significant concerns, particularly in the case of children, as it may potentially lead to neurological and intellectual development challenges.[76] In adults, heightened lead exposure can give rise to health problems, including hypertension, renal impairment, and anemia.

To address this problem, international organizations, such as the World Health Organization (WHO) and the U.S. Environmental Protection Agency have established standards for lead levels in water bodies. WHO's recommendation for drinking water sets a limit of 0.01 mg/L of lead, aiming to safeguard the health of children and pregnant women.[76,77] Ghosh et al. developed a hybrid fiber grating sensor combining high-order long-period grating (LPG) and FBG for the simultaneous detection of Pb^{2+} ions and water temperature.[78] Figure 3(a) illustrates the schematic diagram of a hybrid fiber grating sensor system. The sensor's working principle relies on the strong light–matter interactions between the abrupt field of the high-order cladding modes and the change in the RI of the surroundings caused by the selective adsorption of heavy metal ions. The researchers created a label-free, highly selective Pb^{2+} ion sensor based on LPG by modifying its surface with cross-linked CS and nitrogen-doped graphene oxide-based nanocomposites (CCS-NGO) and PAA polymers using a layer-by-layer electrostatic adsorption method [see Fig. 3(b)]. This modification resulted in a lower detection limit of 0.5 nM in the

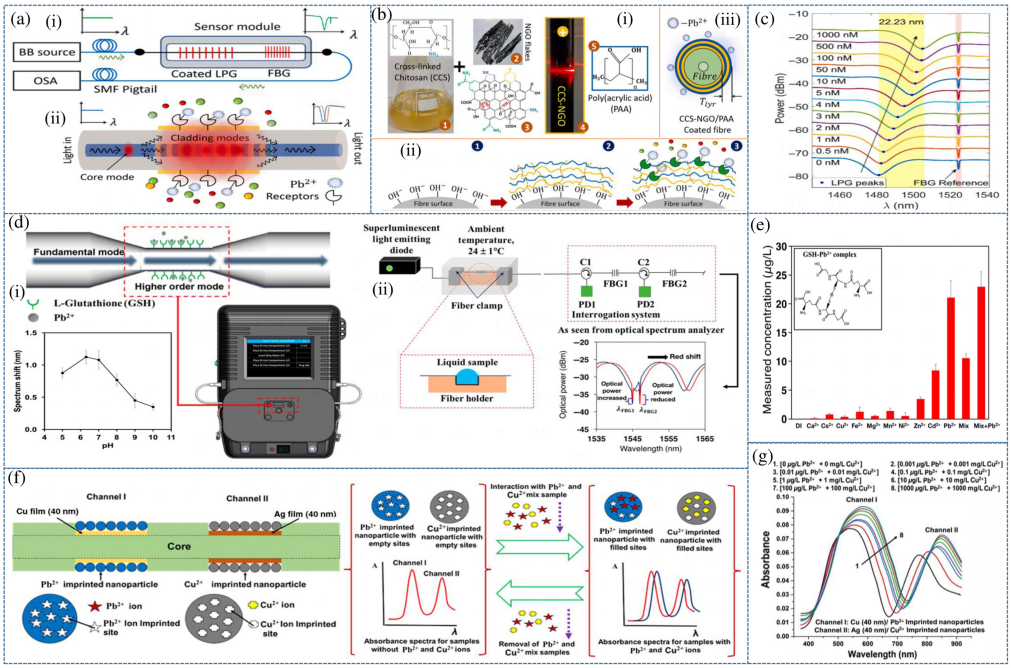

Fig. 3 (a) Schematic diagram of a high-order LPG and an FBG hybrid fiber grating sensor system for simultaneous detection of (i) Pb^{2+} ions and water temperature and (ii) operating schematic diagram of LPG. (b) LPG surface modification materials and their self-assembly characteristics. (c) Spectrogram used for the online monitoring of Pb^{2+} ion concentration (0 to 1000 nM).[78] (d) Schematic diagram of (i) portable optical fiber Pb^{2+} sensing mechanism and (ii) microfiber-sensing platform based on FBG demodulation system. (e) Selectivity.[79] (f) Schematic diagram of fiber structure and principle for the detection of Pb^{2+} and Cu^{2+}. (g) Optical fiber SPR absorption spectrum for the detection of Pb^{2+} and Cu^{2+}.[80]

Pb^{2+} concentration range of 0 to 1000 nM [see Fig. 3(c)]. CS is a linear cationic aminopolysaccharide hydrophilic biosorbent with a high content of active amino ($-NH_2$) and hydroxyl ($-OH$) groups. The crosslinked CS formed a three-dimensional network using an optimized amount of GA, enhancing its stability without compromising its inherent metal adsorption capacity. The interaction between the nitrogen atoms of the amino group and the valence Pb^{2+} ions led to the formation of NH_2 Pb^{2+} complexes. Additionally, water uptake in the CCS-NGO/PAA sensing layer may cause protonation of the amino group and the formation of $-NH_3$, facilitating the ion exchange and adsorption of Pb^{2+} ions on the nitrogen atoms of $-NH_3$. Yap et al.[79] developed a cost-effective and portable Pb^{2+} sensor by utilizing reflected optical power measurements from two FBGs. The surface of the tapered optical fiber-sensing region was coated with a layer of L-glutathione (GSH), which induced a small change in the effective RI when Pb^{2+} bound to the GSH-modified surface.

Figure 3(d) illustrates (i) the portable optical fiber Pb^{2+} sensing mechanism and (ii) microfiber-sensing platform based on the FBG demodulation system. GSH acts as a potent metal chelator, containing glutamate groups of amine and carboxylic acid donors, peptide bonds, and multiple active binding sites in the thiol group, enabling specific recognition of Pb^{2+}. The thiol group in the cysteine residue ($pK4 = 9.65$) exhibits a high affinity at pH 6.5 to 8.3, resulting in the sensor's highest sensitivity at pH 6 to 7. The cysteine residues of GSH can form metal complexes, leading to stronger metal bonds, particularly through thiolate ligands with high affinity for soft metal ions, thereby providing relatively high binding efficiency for Pb^{2+} and excellent selectivity [see Fig. 3(e)]. During actual water sample testing, the GSH-modified microfiber sensor exhibited a slight response to blank samples due to interference from background ions, but this false positive result remained below the Pb^{2+} safety limit. A two-channel optical fiber SPR platform based on the modification with heavy metal ion-imprinted nanoparticles was presented by Shrivastav and Gupta.[80] Figure 3(f) shows the optical fiber structure and principle for the detection of Pb^{2+} and Cu^{2+}. Channel I and channel II are equipped with thin films of copper and silver on the fiber core surfaces, respectively. Subsequently, Pb^{2+} ion-traced nanoparticles and Cu^{2+} ion-imprinted nanoparticles are applied to the surfaces of the respective channels. Channel I is dedicated to detecting Pb^{2+} ions, whereas channel II is employed for detecting Cu^{2+} ions. Figure 3(g) shows the optical fiber SPR absorption spectrum for the detection of Pb^{2+} and Cu^{2+}. The sensitivities of channel I and channel II are 8.19×10^4 nm/(μg/L) and 4.07×10^5 nm/(mg/L), respectively. The sensor exhibits remarkable detection capabilities, with the ability to detect Pb^{2+} and Cu^{2+} ion concentrations as low as 4.06×10^{-12} g/L and 8.18×10^{-10} g/L, respectively. This probe offers simplicity, cost-effectiveness, and selectivity, making it suitable for on-line monitoring of heavy metal ions in water quality. Suhailin et al. introduced a D-type optical fiber SPR sensor for detecting the low concentrations of Pb^{2+} in aqueous solutions.[81] The sensor's configuration involved sputtering an Au film on the D-type fiber surface as a plasma excitation layer, followed by modification with a layer of γFe_2O_3/reduced graphene oxide (rGO) nanocomposites to serve as the sensing layer. The sensor exhibited a Pb^{2+} sensitivity of 1.2 nm/μg/L, and the lower limit of detection was 0.001 ppm. Nazari et al.[82] developed an efficient sulfonated UiO-66(Zr) optical fiber for the rapid Pb^{2+} detection. UiO-66(Zr) metal-organic frameworks (MOFs) functionalized with SO_3H groups [SO_3H-UiO-66(Zr)] was modified on the end face of the optical fiber to detect lead cations in water at 25.2, 43.5, and 64.0 ppm levels. The functionalized MOF was coated on the end face of an SMF, serving as an in-fiber FPI to detect changes in the MOF's optical properties caused by Pb^{2+} adsorption, manifested as wavelength shifts in the interference spectrum. The optical fiber and SO_3H-UiO-66(Zr) material exhibit excellent stability in the pH range of 2 to 9, rendering them suitable for long-term Pb^{2+} monitoring in aqueous environments.

3.1.2 *Mercury*

Mercury (Hg), in the forms of methylmercury and inorganic mercury, is a toxic heavy metal. It can contaminate water through various channels, such as industrial wastewater and coal combustion, eventually entering the human body through the food chain. Prolonged ingestion of high concentration of mercury can lead to detrimental effects on the nervous, immune, and

circulatory systems, and in severe cases, it may impair brain development and intelligence.[83] Accurate detection of Hg^{2+} concentration in water is crucial for monitoring and controlling mercury pollution in the environment, thus safeguarding natural ecosystems and biodiversity.[84] The WHO recommends that the Hg^{2+} concentration in drinking water should not exceed 0.001 mg/L.[85]

Commonly employed optical fiber-sensing methods for Hg^{2+} in water include SPR sensing and fluorescence optical fiber sensing.[86,87] Lu et al. presented a dual-mode detection technique combining plasmon resonance spectroscopy and electrochemistry (EC-SPR) for real-time quantitative detection of Hg^{2+} concentrations with remarkable selectivity and sensitivity.[88] Figure 4(a) shows the schematic diagram of the optical fiber-based EC-SPR sensor structure and system. To achieve this, they first deposited a 3-nm chromium film as a bonding layer onto the polished optical fiber's surface. Subsequently, a 45-nm thick gold film was sputtered on top, followed by the modification of 1,6-hexanedithiol (HDT) to form a monolayer of dithiols on the gold surface, providing additional free thiol groups for sensing. The gold-coated fiber served both as a working electrode for EC sensors and as an extremely sensitive SPR sensor. To enhance Hg^{2+} detection sensitivity, they employed cyclic voltammetry (CV) to activate the HDT-modified gold film electrode. The interaction of Hg^{2+} ions with the free thiol groups on the HDT monolayer led to a significant shift in the SPR wavelength, which was further accelerated and amplified by the CV treatment. The researchers found that multiple CV scans on the HDT monolayer resulted in an increased acceleration of the SPR wavelength shift, ultimately improving the lower limit of Hg^{2+} concentration monitoring from 0.47 to 0.22 μM [see Figs. 4(b) and 4(c)]. Additionally, the CV scans promoted the redox reaction of Hg^{2+} ions, facilitating their detachment from the HDT monolayers. This redox process restored the active sites on the sensor, allowing for effective regeneration. This solution offers great potential for monitoring heavy metal ion concentrations in various applications, including water quality assessment, agricultural irrigation, and drinking water safety.

Yuan et al.[89] developed an OFS for Hg^{2+} detection based on the SPR effect. 4-mercaptopyridine (4-MPY)-functionalized gold nanoparticles (Au NPs/4-MPY) were used as a signal-amplifying tag. 4-MPY was modified on the surface of gold-plated fibers through the formation of an Au-S bond. In this configuration, the pyridine nitrogen becomes exposed to the solution, facilitating its coordination with Hg^{2+}. Initially, Hg^{2+} interacted with 4-MPY assembled on the Au membrane, followed by the capture of Au NPs/4-MPY by Hg^{2+}, resulting in the formation of a sandwich structure comprised of (Au film/4-MPY)-Hg^{2+}-(Au NPs/4-MPY).

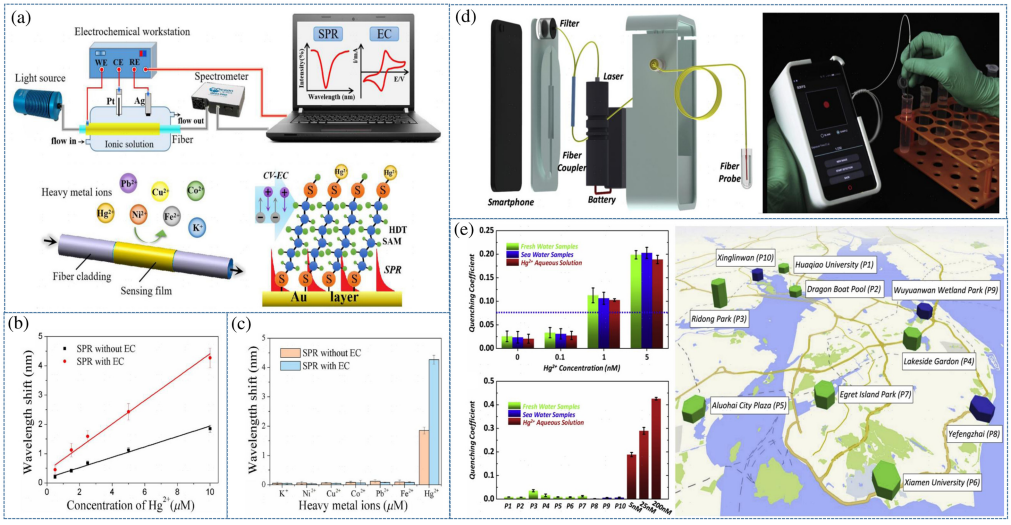

Fig. 4 (a) The schematic diagram of optical fiber-based EC-SPR sensor for Hg^{2+} detection. (b)–(c) The comparison of SPR responses with and without CV treatments;[88] (d) SOFFS hardware design; and (e) applications of SOFFS in the fresh and sea water samples.[47]

The coupling effect between the Au film and the Au NPs produces a strong localized SPR. The sensor was able to detect the Hg^{2+} concentration in the range of 8 to 100 nM with a detection limit of 8 nM. The practicality of the sensor for Hg^{2+} detection in tap water samples was also verified. Liu et al. designed an SOFFS for long-range, real-time online quantitative determination of Hg^{2+} concentration using fluorescence burst method.[47] The handheld sensor incorporates a built-in power supply, enabling rapid Hg^{2+} concentration detection in just 3 min, which includes the replacement of the optical fiber probe, fluorescence image recording, and data analysis. The sensor's operation is straightforward and efficient. It consists of a semiconductor laser for exciting the fluorescence signal, a quantum dot-modified optical fiber probe for Hg^{2+} sensing, and a smartphone equipped with a filter for acquiring the fluorescence signal, as shown in Fig. 4(d). Upon verifying SOFFS's performance, it was employed for Hg^{2+} detection in both freshwater and seawater environments, using water samples with a pH of ~7, Fig. 4(e) shows the applications of SOFFS in the fresh and sea water samples. Notably, SOFFS boasts an ultralow detection limit of 1 nM and an extensive detection range spanning from 1 to 1000 nM for Hg^{2+} concentration.

3.1.3 *Cadmium*

Cadmium (Cd), primarily originating from battery manufacturing, mining activities, and industrial wastewater, is a profoundly toxic metal. Once it enters water, cadmium can contaminate water sources through bioaccumulation and sedimentation, posing a threat to ecological equilibrium. Long-term exposure to cadmium can lead to health problems, such as kidney damage, osteoporosis, and cancer.[90] In accordance with WHO standards, the cadmium concentration in drinking water should not exceed 0.01 mg/L. Cai et al. developed an exceptionally sensitive plasma fiber probe by utilizing a gold-plated tilted fiber Bragg grating (TFBG).[91] *Acinetobacter* spp. bacteria were modified on the surface of the gold film, allowing for the precise determination of cadmium ion (Cd^{2+}) concentration in a solution. Figures 5(a)–5(c) show the Cd^{2+} detection principle and performance based on a gold-plated TFBGs. The detection limit for Cd^{2+} was impressively close to 1 ppb, and the detection process was achieved within a rapid 10-min timeframe. Li et al.[92] developed a high-precision Cd^{2+} sensor based on a twisted helical fiber (THF). The sensor incorporates a propylene thiourea membrane modification on the surface of the twisted fiber, resulting in the formation of a cross-linked "-S-Cd-S-" structure with Cd^{2+}. The twisted fiber structure and sensing mechanism are depicted in Figs. 5(d) and 5(e), wherein

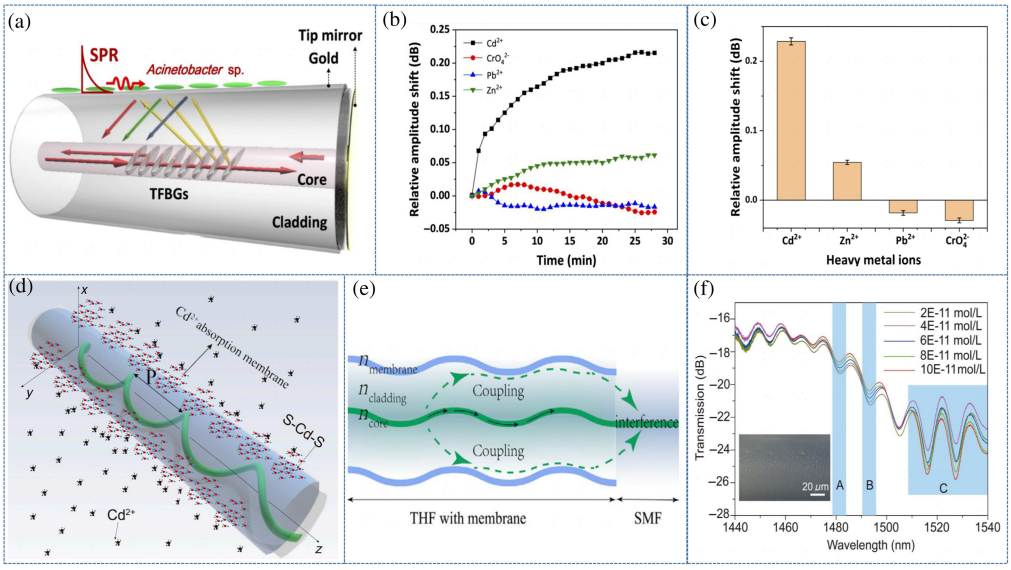

Fig. 5 (a) SPR excitation with TFBGs; (b) time response plot of heavy metal ion detection; (c) selectivity at the same concentration of 10 ppb;[91] (d) the sensing structure and (e) mechanism of THF-based sensor; and (f) transmission spectra in Cd^{2+} concentration detection.[92]

the twisting effect allows light in the core to leak into the cladding. Consequently, part of the light propagates forward along the core, while another part leaks into the cladding, reflects back to the core, and the two optical paths exist simultaneously. This coupling and interference occur within an SMF, leading to multiple resonance depressions, as illustrated in Fig. 5(f). The prepared band film THF demonstrates high sensitivity, achieving 0.07252 nm/$(10^{-11}$ mol/L) in wavelength modulation and 0.08975 dB/$(10^{-11}$ mol/L) in amplitude modulation. Furthermore, dual-wavelength modulation can be achieved through dual-mode calibration, which significantly enhances the accuracy of Cd^{2+} concentration monitoring.

3.2 Microbial Surveillance

Microorganisms in water comprise bacteria, algae, fungi, and viruses. Among these, bacteria are prevalent in various water bodies. Certain bacteria play crucial roles, such as decomposing organic matter and participating in nitrogen cycling, while pathogenic bacteria, such as *E. coli* and *Salmonella*, can cause water contamination and waterborne diseases.[93,94] *Escherichia coli* (*E. coli*), a group of intestinal bacteria, is frequently employed as an indicator microorganism for assessing water body contamination levels.[94] The detection of *E. coli* can reveal the existence of fecal contamination, consequently determining whether a water is contaminated with pathogenic microorganisms.[95] Kaushik et al.[96] designed an *E. coli* sensor based on the optical fiber SPR effect. Molybdenum disulfide (MoS_2) nanosheets were linked to the gold-coated optical fiber via Au-S bonds, and *E. coli* monoclonal antibodies were attached to the MoS_2-functionalized sensing surface through hydrophobic interactions, enabling precise, specific, and rapid (∼15 min) label-free detection of *E. coli*. Figure 6(a) depicts the diagram of the optical fiber SPR immunoassay system designed for detecting *E. coli*, whereas Fig. 6(b) illustrates the *E. coli* sensing performance both with and without MoS_2 sensitizing layer. Nevertheless, the

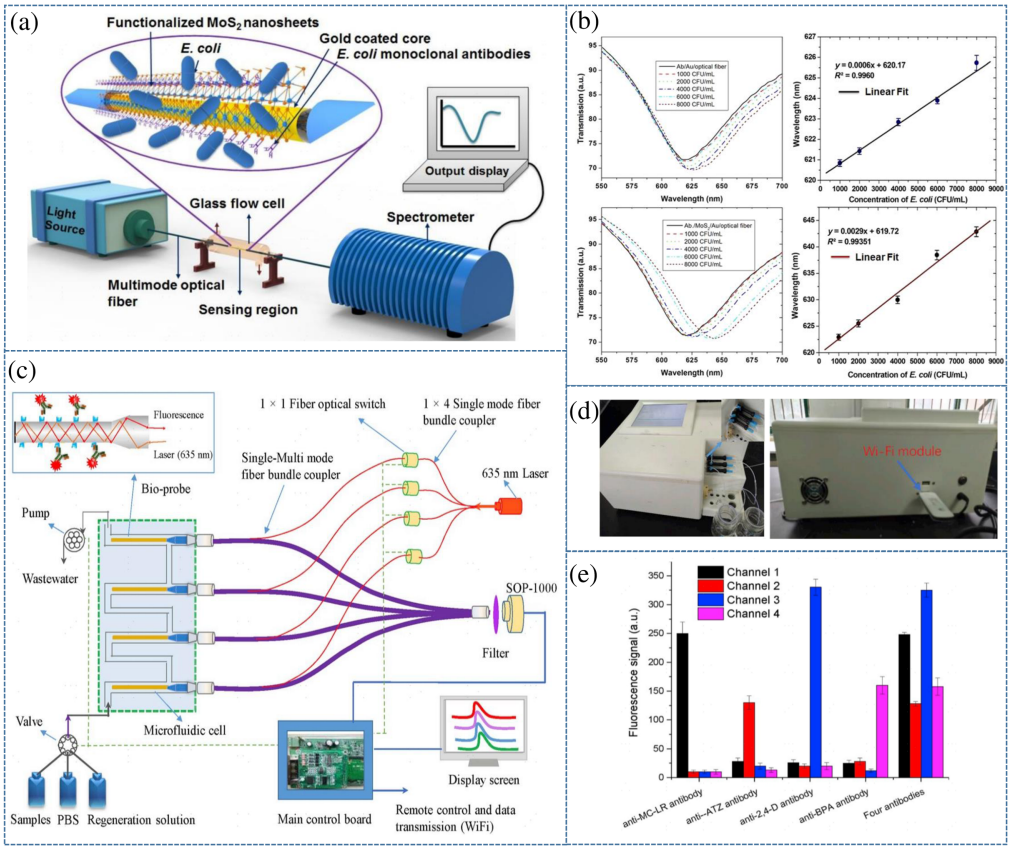

Fig. 6 (a) Diagram of optical fiber SPR *E. coli* immunodetection system; (b) *E. coli* sensing performance with/without MoS_2 sensitizing layer;[96] (c) fabrication of the fluorescence microarray biosensing platform (FMB) system; (d) the forward and back photo of the FMB system; and (e) the fluorescence intensities of four channels.[97]

practical utility of this system is hampered by the decline in sensor performance stemming from the instability of *E. coli* antibodies. Kaushik et al.[98] developed an immunosensor for label-free detection of *Escherichia coli* based on cascaded chirped LPGs. It works in a manner similar to a MZI, where the resonance wavelength is shifted by changing the RI of the intergrating space region without affecting the actual grating region. The limiting bandwidth of the interference fringes improves the resolution of the resonance wavelength analysis of transmission spectra. The proposed immunosensor is capable of selectively detecting *E. coli* in real samples including lake water. Halkare et al.[99] developed an *E. coli* immunosensor based on wild-type phage T4 as a biorecognition element. Bacteria (analytes) were first immobilized on the sensing surface, followed by phage exposure for specific bacteria detection. The key advantage of this approach is that phages can freely diffuse and orient themselves, efficiently binding to the bacterial surface immobilized on the sensing platform. This sensing strategy finds extensive applications in the specific detection of bacterial species in environmental samples.

The detection of microcystins in water is of paramount importance. Microcystins are highly toxic compounds produced by certain cyanobacteria, such as cyanobacteria or microcystis. Elevated levels of microcystins in water can trigger a cyanobacterial bloom, commonly known as an algal bloom outbreak, resulting in a significant decline in water quality. Prolonged exposure to high microcystins concentrations in water may lead to poisoning or even the death of fish and other aquatic organisms. Moreover, human exposure to microcystin-contaminated water can cause gastrointestinal problems, skin irritation, and neurotoxic effects. Long et al.[97] developed a portable automated fluorescence microarray biosensing (FMB) platform for microcystin-LR (MC-LR) sensing. Figure 6(c) depicts the fabrication of the FMB platform system. Through the control of optical fiber switches, only one excitation light and a photodiode detector can achieve four-channel parallel fluorescence analysis, making it suitable for real-time parallel monitoring of various analytes. The front and back photo of the FMB system is shown in Fig. 6(d). The optical structure of the FMB significantly enhances light transmission and fluorescence collection efficiency, resulting in improved detection sensitivity. Figure 6(e) depicts the fluorescence intensities of four channels in the FMB. Moreover, fewer optical separators and the elimination of strict optical alignment contribute to the system's compactness and portability. As a multiplexed, portable, rapid, and quantitative detection platform, the FMB holds promise for early warning of contaminants in pollution incidents and water quality management. Yang et al.[100] developed a portable optical fiber chemiluminescence biosensor (FOCB) system. They utilized an optical fiber bioprobe, modified with hapten-carrier protein conjugates as the biorecognition element. The detection of MC-LR was achieved through an indirect competitive sandwich chemiluminescence immunoassay, demonstrating high sensitivity for MC-LR. The detection limit of MC-LR was 0.03 g/L under the optimal conditions.

Optical fiber-sensing techniques in water quality environments mainly include SPR, fluorescence, and interferometric techniques. These sensing technologies offer several advantages, such as high sensitivity, real-time monitoring, non-invasiveness, and remote control. These advantages play a crucial role in effectively monitoring the concentration and contamination of heavy metal ions and microorganisms in water. Table 1 illustrates the comparative performance of OFSs for heavy metals in water quality. Table 2 illustrates the comparative performance of OFSs for microorganisms in water quality.

4 Air Quality Monitoring

4.1 Nitrogen Oxides

Nitrogen oxides (NO_x) are widely recognized as one of the primary air pollutants, and frequent exposure to these highly reactive gases can lead to various health problems.[108,109] Nitric oxide, a colorless and odorless gas, is insoluble in water. Its production can be categorized into two types: enzymatic nitric oxide and non-enzymatic nitric oxide. Due to its association with free radicals, nitric oxide exhibits high reactivity and paramagnetic properties. When reacting with oxygen, it transforms into the corrosive gas nitrogen dioxide (NO_2).

NO_2 appears as a red-brown gas at room temperature and can readily dissolve in water, resulting in the formation of nitrous acid and nitric acid. NO_2 has a strong irritant effect on human eyes and respiratory organs, leading to symptoms such as cough, yellow phlegm,

Table 1 Overview of optical fiber sensors for heavy metals in water quality.

Analytes	Method	Sensing layer	Sensitivity	Detection range	LOD	References
Pb^{2+}	Hybrid fiber grating (LPG + FBG)	CCS-NGO/PAA	2.547 nm/nM	0 to 1000 nM	0.5 nM	78
Pb^{2+}	Tapered fiber + FBG-based interrogation system	L-glutathione	—	0 to 50 μg/L	5 μg/L	79
Pb^{2+} and Cu^{2+}	Unclad highly multimode plastic clad silica (PCS) fiber	Pb^{2+} imprinted nanoparticles/ Cu^{2+} imprinted nanoparticles	Pb^{2+}: 8.19×10^{4} nm/(μg/L) and Cu^{2+}: 4.07×10^{5} nm/(mg/L)	Pb^{2+}: 0 to 1000 μg/L, Cu^{2+}: 0 to 1000 mg/L	Pb^{2+}: 4.06 pg/L and Cu^{2+}: 81 pg/L	80
Pb^{2+}	D-shaped MMF	Au/γFe_2O_3/rGO	1.2 nm/μg/L	0.001 to 15 ppm	0.001 ppm	81
Pb^{2+}	FPI	SO_3H-UiO-66(Zr)	—	25.2 to 64.0 ppm	25.2 ppm	82
Hg^{2+}	optical fiber-based EC-SPR	1,6-hexanedithiol	—	0.5 to 10 μM	0.22 μM	88
Hg^{2+}	Tapered fiber fluorescence	CdSe/ZnS QDs	—	0 to 1000 nM	1 nM	89
Hg^{2+}	Unclad optical fiber SPR	(Au film/4-MPY)-Hg^{2+}-(AuNPs/4-MPY) sandwich	—	8 to 100 nM	8 nM	47
Hg^{2+}	TFBG-SPR-AuNPs	T-Hg-T structure	/	10 pM to 1 mM	3.073 pM	101
Hg^{2+}	LSPR-based U-bend fiber	CS/Au NPs	—	0.1 to 540 ppb	/	102
Hg^{2+}	Optical (eFBG)	CNC-bolaamphi-phile	—	1 pM to 10 nM	1 pM	103
Cd^{2+}	Au-TFBGs	*Acinetobacter* spp.	/	0.1 to 1000 ppb	1 ppb	91
Cd^{2+}	Twisted fiber	propylene thiourea ((S–Cd–S))	0.7252 nm/pM; 0.8975 dB/pM	20 to 80 pM	—	92
Cd^{2+}	Air-hole-assisted multicore microstructured optical fiber	Allyl thiourea (S–Cd–S)	7.443×10^{9} nm/(mol/L)	20 to 120 pM	6 pM	104
Cd^{2+}	U-shaped optical probe	PVA-CS/AuNPs	0.028 intensity/ppb	1 to 20 ppb	800 ppt	105

Table 2 Overview of optical fiber sensors for microorganisms in water quality.

Analytes	Method	Sensing layer	Sensitivity	Detection range	LOD	References
E. coli	MMF	$AuMoS_2$/*E. coli* antibodies	2.9 nm/1000 CFU mL^{-1}	1000 to 8000 CFU/mL	94 CFU/mL	96
E. coli	Chirped-LPG	Anti-*E. coli* antibodies	—	10 to 60 CFU/mL	7 CFU/mL	98
E. coli B40	Ubent optical fiber probes LSPR	AuNPs-*E. coli* B40-Bacteriophage T4	/	10^3 to 10^7 CFU/mL	216 CFU/mL	99
E. coli	Etched-LPG fiber	Bacteriophage T4/TiO_2	2.55 nm/RIU	0 to 50 CFU/mL	10.05 ppm	106
MC-LR	Fluorescence microarray biosensing platform	MC-LR-OVA	—	0 to 1000 μg/L	0.04 μg/L	97
MC-LR	U-bent fibers	Polyaniline/anti-MC LR antibodies	—	0.1 to 1000 ppb	0.1 μg/L	107
MC-LR	FOCB	MC-LR-OVA	—	0.23 to 190 μg/L	0.03 μg/L	100

breathing difficulties, and, in severe cases, even pulmonary edema, ultimately leading to death. When the air's nitrogen dioxide concentration reaches 0.006%, individuals may experience sore throat, cough, and lung pain in a short period. At 0.01% concentration, strong coughing, vomiting, and nerve paralysis may occur rapidly. A concentration of 0.025% of nitrogen dioxide can prove fatal quickly. In addition to natural sources, NO_2 mainly originates from fuel combustion, urban vehicle exhaust, industrial production processes, and lightning discharges. It is a significant contributor to acid rain and plays a major role in the formation of photochemical smog. Detecting, eliminating, and preventing air pollution are crucial for maintaining air quality standards. Given the adverse health effects of nitrogen dioxides, continuous monitoring, and quantitative detection of these gases at trace levels are essential to control exposure to these pollutants effectively.[22,110,111] Reliable sensors for measuring nitrogen oxides concentrations are of utmost importance in this regard.

Zou and Wang[112] proposed an optimized long path differential optical absorption spectrometry (LPDOAS) system with enhanced UV light intensity, enabling the simultaneous quantification of SO_2 and NO_2. In contrast to conventional configurations employing telescope mirrors, this system adopted a Y-type optical fiber structure. The maximum calibration errors for SO_2 and NO_2 were 4.19% and 5.22%, respectively, with the combined error for both gases was falling well below 10%. The real-time measurement of SO_2 and NO_2 demonstrated strong alignment with the data recorded at monitoring stations, both in order of magnitude and variation trends. Laboratory calibration and field measurements confirmed the effectiveness of online air pollution monitoring based on optical fiber LPDOAS. Peng et al.[113] used spectrum superposition theory to decompose the NO differential optical density from the gas mixture, enhancing the system's selectivity by overcoming cross-sensitivity to SO_2 and NO in band-I. The achieved detection limits were 60 ppb for SO_2 and 7 ppb for NO, with non-linear deviations of 0.79% FS and 0.47% FS for SO_2 and NO, respectively. The system employed optical fiber as the signal transmission medium for gas detection. Sangeetha and Madhan[22] designed and fabricated a MoS_2/graphene-based hybrid sensor, evaluating its gas sensing performance for various gases (ethanol, methanol, acetone, CO, NO_2, and formaldehyde) using a clad-removed optical fiber method. Figure 7(a) depicts the experimental setup for the optical fiber clad-modified gas sensor. Mohanraj et al.[114] demonstrated an all fiber-optic multigas (FOMS) (NH_3, NO_2, and CO) sensor by coating synthesized molybdenum tungsten disulfide ($MoWS_2$) nanosheets on a side-polished fiber (SPF). The $MoWS_2$-coated SPF sensor was used for sensing three hazardous gases: NH_3, NO_2, and CO. Figure 7(b) illustrates the diagram of the all FOMS sensor with the $MoWS_2$ sensitizing layer.

Theoderaj et al.[24] fabricated a clad-modified OFS, coating CdS over the clad-modified region using chemical bath deposition as the NO_2 gas-sensing medium. Figure 7(c) illustrates the gas sensing mechanism of the CdS-coated clad-modified OFS. Yao et al.[115] implemented a 2D near-infrared plasmonic tungsten oxide (WO_x)-enabled ultrasensitive optical fiber gas sensor on a side-polished D-shape single-mode optical fiber. Figure 7(d) displays the gas sensing response of the 2D WO*x*-based OFS. A fluorescent probe composed of carbon quantum dots with o-phenylenediamine groups was prepared by the microwave method to selectively detect NO.[117] Mechery and Singh[116] designed two types of reflective optical fiber-sensing probes based on the signal transduction mechanism of spectral changes at the nanopore of sol–gel elements. The extrinsic design utilized the optical fiber transflection probe geometry with its sensor element placed at the distal end of the fiber bundle. The nitrogen dioxide-mediated coloration reaction ensured high specificity of detection when tested in a mixture of gas samples. Figure 7(e) shows the schematic of the experimental setup used for the two different OFS designs for the detection of trace amounts of NO_2 in a mixture of gases. Niu et al.[118] prepared a fibrous rGO/MoS_2 composite through a wet-spinning and a hydrothermal method.

4.2 Carbon Monoxide

Under normal conditions, carbon monoxide (CO) is a colorless, odorless, and tasteless toxic gas, which is also insoluble in water, rendering it a neutral gas. When inhaled with air, CO enters the bloodstream through the alveoli and combines with hemoglobin to form carbon oxygen hemoglobin (HbCO). This compound is difficult to decompose and hinders the blood's ability to carry oxygen, leading to hypoxia. Moreover, HbCO not only fails to transport oxygen itself but also

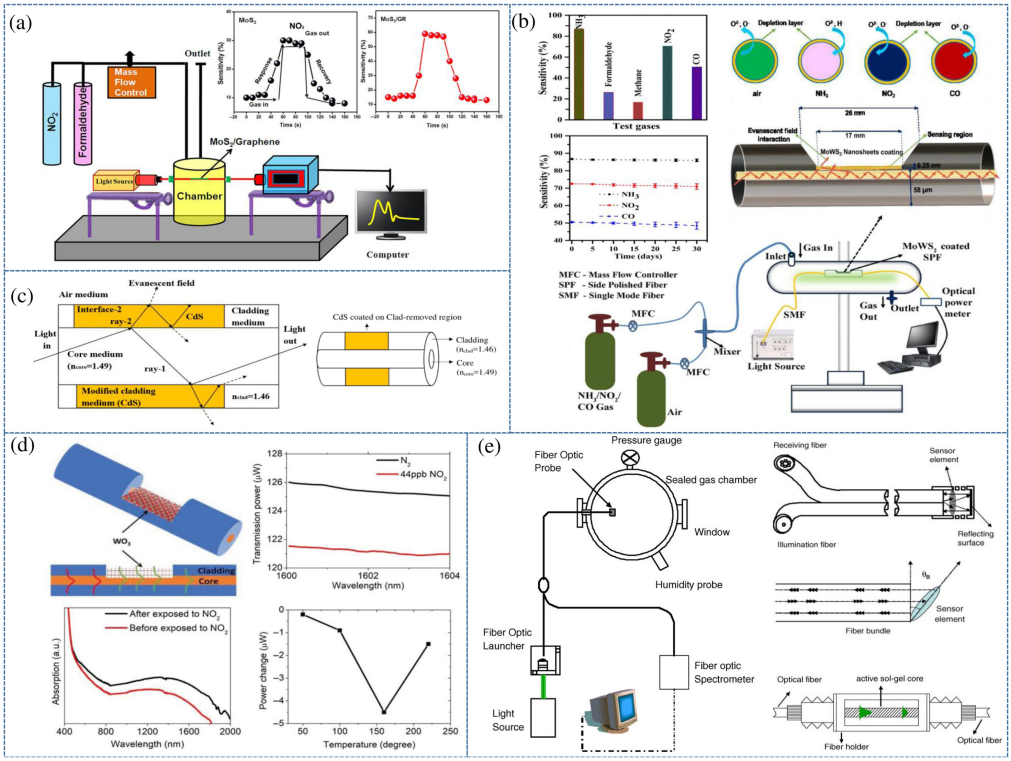

Fig. 7 (a) The diagram of the experimental setup for the optical fiber clad-modified gas sensor.[22] (b) Diagram of the all FOMS (NH_3, NO_2, and CO) sensor with the $MoWS_2$ sensitizing layer.[114] (c) Gas sensing mechanism of the CdS-coated clad-modified optical fiber sensor.[24] (d) Gas sensing response of the 2D WO*x*-based optical fiber sensor.[115] (e) Schematic of the experimental setup used for two different optical fiber sensor designs for the detection of trace amounts of NO_2 in a mixture of gases.[116]

interferes with the dissociation of HbO_2, causing double hypoxia in the tissues. Consequently, tissue hypoxia and carbon dioxide retention ensue, resulting in the manifestation of oxygen toxicity symptoms. The carbon atom within the CO molecule exhibits a +2 oxidation state, susceptible to further oxidation to +4. Thus the imperative quest for real-time, quantitative, and accurate CO gas detection remains paramount.[119,120]

Peng et al. developed an optical fiber dual F–P interferometric CO gas sensor by coating a PANI/Co_3O_4/GO (PCG) sensing membrane on the end face of the optical fiber. The FPI sensor was created by splicing one end of endlessly photonic crystal fiber (EPCF) with an SMF and applying the PCG sensing membrane to the other end. This sensor offers compact size, cost-effectiveness, high sensitivity, strong selectivity, and a simple structure, making it suitable for detecting low concentrations of CO gas.[121] Figure 8(a) illustrates the structural diagram of the FPI sensor, where a section of EPCF with a core RI of n_{EPCF} is spliced to a conventional SMF with a core RI of n_{SMF}. Zhou et al.[122] proposed and fabricated a Michelson interferometric CO OFS based on Co/Ni-MOF-74, a bimetallic-ion-coordination MOFs material, using the solvothermal method. Figure 8(b) presents the diagram of the Michelson interferometric optical fiber CO sensor with Co/Ni-MOF-74 as the sensitizing layer. He et al.[123] developed a CO sensor based on a Michelson interferometer combined with α-Fe_2O_3/reduced graphene oxide quantum dots (rGOQDs) composite film. Figure 8(c) depicts the diagram of a Michelson interferometric optical fiber CO sensor employing α-Fe_2O_3/rGOQDs as the sensitizing layer. Chen et al. successfully developed an innovative optical fiber-based intensity-modulated CO gas sensor, utilizing a cerium dioxide (CeO_2) sensing film applied to a thin-core fiber (TCF). The sensor structure includes symmetrically spliced SMF, no-core fiber (NCF), and TCF, forming an SMF-NCF-TCF-NCF-SMF Mach–Zehnder interference configuration.[124]

Figure 8(d) illustrates the diagram of the intensity-modulated CO gas sensor with the CeO_2 film. Yao et al.[125] developed the first CO photothermal sensor using a hollow core negative

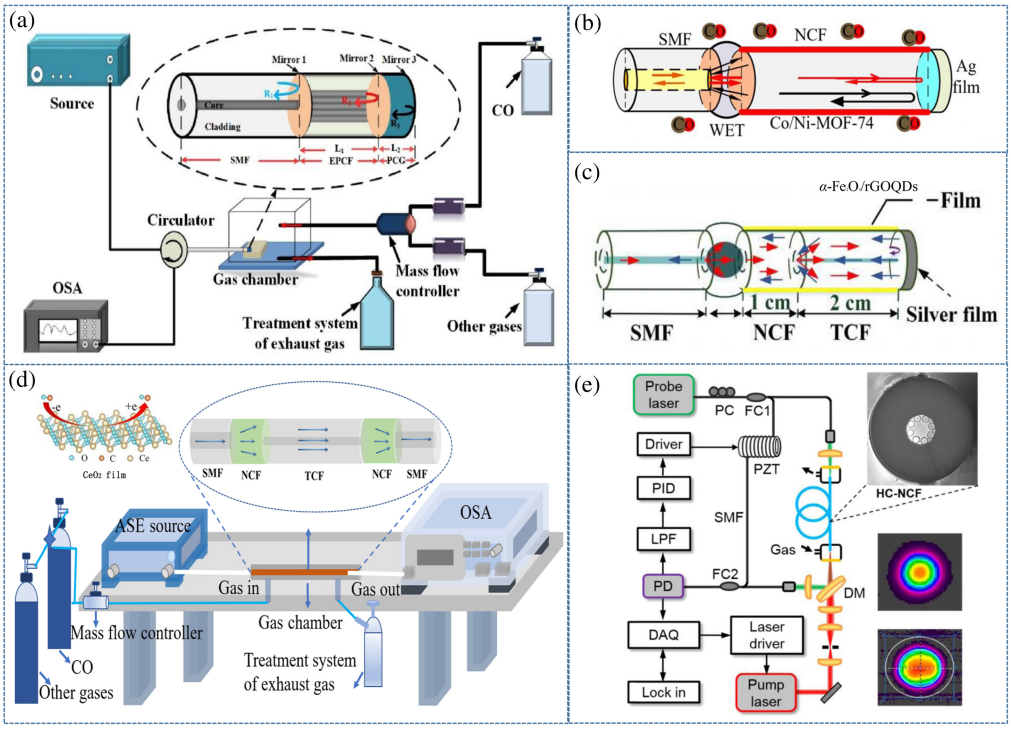

Fig. 8 (a) Diagram of the dual FPI sensor and the corresponding experimental setup.[121] (b) Michelson interferometric optical fiber CO sensor with the Co/Ni-MOF-74 sensitizing layer.[122] (c) Michelson interferometric optical fiber CO sensor with the α-Fe_2O_3/rGOQDs sensitizing layer.[123] (d) Intensity-modulated CO gas sensor with the CeO_2 film.[124] (e) Experimental setup of the PTI CO sensor using a HC-NCF.[125]

curvature fiber (HC-NCF), effectively enhancing the photothermal signal by incorporating a water vapor additive. Figure 8(e) displays the experimental setup of the PTI CO sensor utilizing a HC-NCF. Liu et al. introduced a rapid gas sensing scheme based on non-dispersive frequency comb spectroscopy (ND-FCS) capable of measuring multiple gas components. The researchers experimentally investigated its capacity for multicomponent gas measurement using the time-division-multiplexing (TDM) method to achieve specific wavelength selection of the fiber laser optical frequency comb. With TDM, the quasi-synchronous dynamic measurement of the three gases was achieved. The proposed ND-FCS exhibits exceptional sensing ability without the need for low-efficiency spectrum scanning and complex laser mode locking configuration, making it a promising candidate for long-term, high sensitivity, fast response gas sensing applications and multicomponent measurement requirements.[126]

4.3 Volatile Organic Compound

VOCs constitute a group of organic substances known for their high vapor pressure at room temperature. They readily evaporate into the air, giving rise to flammable and explosive mixtures. Commonly encountered VOCs include benzene, formaldehyde, acetone, xylene, and ethyl acetate, finding applications in various industrial processes, building materials, household products, cosmetics, and cleaning agents. Long-term exposure to elevated levels of VOC pollution may result in various health issues, including headaches, breathlessness, and eye irritation.[127,128] Furthermore, specific VOCs are associated with chronic respiratory diseases and neurological problems. Thus it becomes imperative to closely monitor VOC levels. To address this, OFSs emerge as the most promising gas detection devices. Their compact size, high sensitivity, resistance to electromagnetic interference, and ability to withstand harsh environments make them ideal for VOC monitoring applications.[16,17,129]

Benzene, a colorless and transparent liquid with a distinct aromatic odor, finds extensive applications as a solvent and chemical raw material, despite its profound toxicity and hazardous nature. It poses serious threats to the human nervous and immune systems, the WHO

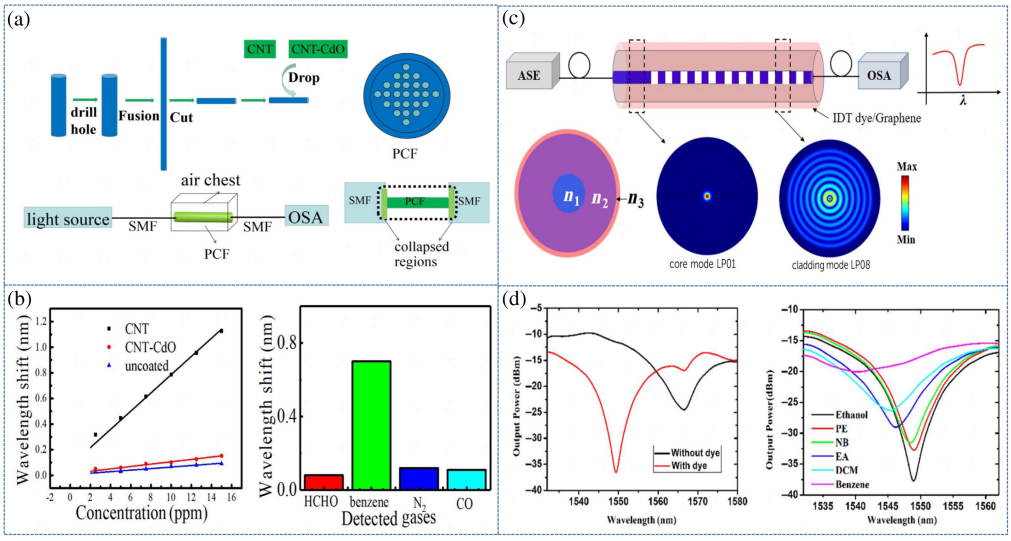

Fig. 9 (a) MZI photonic crystal optical fiber benzene sensor based on CNT modification. (b) Concentration and specificity test plots of benzene sensors.[130] (c) Graphene/IDTC1-modified long-period optical fiber grating benzene sensors. (d) Transmission spectra in the presence or absence of IDTC1 dye and in different gas atmospheres.[131]

recommends maintaining airborne benzene concentrations below 5 ppm for an 8-h average. Wang et al.[130] developed a photonic crystal OFS utilizing the MZI, as shown in Fig. 9(a). The sensor incorporated a silicon fiber array as the fiber cladding, air holes as the core, and carbon nanotubes (CNTs) as the coating material. Figure 9(b) displays the spectral response of the sensor at various concentrations, wavelength variation for different materials, and specificity. The study revealed that CNTs exhibited a more pronounced response to benzene (0.8 nm/10 ppm) compared to other gases due to $\pi - \pi$ conjugation between the CNTs and the benzene ring, which enhances their selectivity for benzene. The structural features of CNTs (sp2 hybridization) create a conjugated system with the benzene ring's off-domain π-electronic structure, leading to increased benzene adsorption. Dong et al.[131] designed and fabricated a long-period fiber grating sensor with graphene/IDTC1 as the sensitive fiber cladding for quantitative detection of benzene vapor. Figure 9(c) illustrates the schematic diagram of the sensing device and the optical fiber interface. Figure 9(d) exhibits the transmission spectra in the presence or absence of IDTC1 dye and in different gas atmospheres. The sensor demonstrated quantitative benzene detection over a broad dynamic range (20 to 23,000 ppm) and exhibited high sensitivity (0.36 pm ppm^{-1}). Benzene-induced discoloration caused a change in the IDTC1 film's RI on the optical fiber, leading to a shift in the resonance center's wavelength of the long-period fiber grating.

Acetone is a colorless, flammable, and volatile organic solvent. In high concentrations, its vapors can form flammable mixtures with air, presenting a risk of fire and explosion. Pawar et al.[132] developed a dual-cavity F–P interferometric sensor that utilizes graphene/PMMA composite-modified polarization maintaining fibers (PMFs) to detect various volatile gases. The remarkable properties of graphene, such as its RI change, combined with the swelling of PMMA polymer and the effective RI change and swelling of graphene/PMMA composites, make these composites highly appealing for the detection of various VOCs, including acetone, chloroform, toluene, methanol, ethanol, and isopropanol. Bhise et al.[133] introduced an optical acetone detector based on a palladium-modified WO_3 nanostructure (Pd@WO_3) with high sensitivity and reproducibility across a wide concentration range of 20 to 1000 ppm. Table 3 illustrates the comparative performance of OFSs for gases.

5 Conclusions and Prospects

Since the 21st century, the relationship between human beings and environmental resources has become increasingly tense, and the most obvious problem is water pollution and air pollution.

Table 3 Overview of optical fiber sensors for gases.

Gas	Method	Sensing layer	Response/recovery time	Sensitivity	Detection range	LOD	References
$NH_3/NO_2/CO$	SPF	MoS_2 and WS_2	21/60 s; 42 /71 s; 93 s /56 s	86%, 72%, 48%	0 to 500 ppm	—	114
NO_2	D-shaped fiber	2D WO*x*	3.5 min	—	0.044 to 0.176 ppm	8 ppb	115
NO_2	Multimode PCS fibers	SFA and DMNA	30 min	—	1 to 8 ppm	1 ppm	116
$NO_2/N_2/NH_3$	Optical fiber	rGO/MoS_2 composites	5 min	—	50 to 1000 ppm	53 ppb	118
CO	PCG + PCF + SMF	PANI/Co_3O_4/GO (PCG)	—	0.3473 dB m/ppm	—	0.153 ppm	121
CO	HC-NCF	—	30 s	—	0% to 0.13%	0.4 ppm	134
CO	Photothermal interferometry (PTI)	—	10 min	4.4×10^{-8} cm^{-1} $WHz^{-1/2}$	0.64%	0.75 μV ppm	125
CO	SMF-NCF-TCF-NCF-SMF	CeO_2	40/47 s	0.03224 dB/ppm	0 to 70 ppm	0.07630 ppm	124
$NH_3/CO/CO_2$	ND-FCS	—	NH_3: 20 s; CO: 1.2 s; CO_2: 1.2 s	—	NH_3: 0% to 1%; CO: 0% to 20%; CO_2: 0% to 10%	NH_3: 0.0048%; CO: 0.1869%; CO_2: 0.0467%	126
CO/N_2	NCF	Ag/Co/Ni-MOF-74	90/110 s	0.02235 dB/ppm	0 to 35 ppm	1.99046 ppm	122
CO	MI	Ag/α-Fe_2O_3/rGOQDs	70/100 s	0.057 dBm/ppm		105 ppb	123
Benzene	SMF-PCF-SMF	CNT	~100/ ~ 75 s	0.8 nm/10 ppm	—	—	130
Benzene	LPFG	Graphene/IDTC1	60/10 s	0.36 pm ppm^{-1}	20 to 23 000 ppm	—	131
Benzene	Absorbance	$CeO_2 - SnO_2$	51/37 min	−79 counts /ppm	—	—	135
Benzene	MI	No sensing film	—	0.015 pixels/ppm	964 to 19,290 ppm	—	136
Acetone	SMF-PMF	Graphene/PMMA	48 to 52 s/8 to 12 s	11.62 ± 0.0008 pm/(μL/L)	5 to 200 μL/L	1.72 μL/L	132
Acetone	FPI	PDMS	30/8 s	9.1 pm/ppm	5 to 200 ppm	2.19 ppm	137
Acetone	Absorbance	Pd@WO_3	—	80 Normalized response/ppm	20 to 1000 ppm	—	133
Acetone	SMF-ECG-SMF	—	180 s/	−31 pm/ppm	—	—	138
Acetone	LPG	ZIF-8	—	0.015 ± 0.001 nm/ppm	49 to 543 ppm	6.67 ppm	139

With the acceleration of the industrial process and the improvement of people's awareness of the precious environmental resources, people pay more and more attention to water quality testing and air quality monitoring. Optical fiber sensing is one of the most rapidly developing sensors in the 21st century, because of its small size, light weight, easy to bend, anti-electromagnetic interference, anti-radiation performance, and other unique properties, which has been widely used in industry, communications, medical testing, environmental monitoring, and other fields. Combining water quality detection and air quality monitoring with optical fiber-sensing technology is an important research topic in the new era.

Optical fiber-sensing technology offers exceptional analytical performance, reliability, and environmental adaptability in both water quality and air quality monitoring. In terms of sample analysis performance, optical fiber-sensing technology has high sensitivity and high resolution and can detect trace contaminants and pollution indicators in water and air. It enables real-time monitoring and can provide immediate data and information to help respond to and manage environmental pollution problems in a timely manner. In terms of reliability, OFSs use optical principles for measurement and are not affected by electromagnetic interference and electrical noise, so they have high stability and reliability. The structure of the sensor is simple and not easy to be disturbed by mechanical vibration and temperature change and can be operated stably for a long time, providing reliable data support for long-term monitoring. In terms of environmental adaptability, optical fiber-sensing technology is flexible and can be adapted to different environmental requirements through rational design and selection of sensor materials, sensing mechanisms, and sensor arrangement. OFSs can be deployed remotely and are suitable for monitoring tasks in different locations and complex environments.

Furthermore, the simplicity of sample collection and processing, without direct contact, eliminates sample contamination and damage. However, there are still many core technologies to be studied, such as further improving the stability of OFSs, extending the service life, improving the sensitivity and so on.

OFS exhibits certain limitations that warrant attention in future research endeavors. (1) Enhanced sensitivity and detection precision: future work should focus on exploring more stable and reliable fiber structures. This can be achieved through a strategic combination of sensitive film materials and optimizing system signal demodulation accuracy, resulting in an overall improvement in the sensitivity and detection accuracy of optical fiber sensors. (2) Specific detection: the challenges associated with pollution in both water and air environments stem from a variety of substances. To address this, research should aim to devise methods for detecting specific substances within these environments effectively. (3) Multiparameter intelligent detection: the development of an extensive optical fiber sensor network, coupled with wireless data transmission technology, will facilitate multiparameter, large-scale, real-time online intelligent environmental health monitoring. (4) Packaging and protection of sensing probes: the requirement to immerse in water or air environment for extended periods to facilitate online real-time environmental health monitoring underscores the critical significance of preserving the integrity and stability of the minuscule sensing unit. These factors hold substantial sway over the sensing system's performance and durability. Furthermore, sustaining long-term health monitoring in water or air environment without compromising the sensing unit's integrity or sacrificing detection sensitivity represents a pivotal avenue of future research. In summary, optical fiber-sensing technology offers exceptional analytical performance, reliability, and environmental adaptability in water and air quality monitoring. This technology stands as a pivotal resource for accurate, efficient, and enduring environmental monitoring and management.

Disclosures

The authors declare no competing financial interest.

Code and Data Availability

The data utilized in this study were obtained from Web of Science. Data are available from the authors upon request and with permission from the corresponding publisher.

Acknowledgments

This research was funded by the National Natural Science Foundation of China (Grant No. 62205118) and the Major Science and Technology Project of Hubei Province of China (Grant No. 2023BCA003).

References

1. Z. Liu et al., "Multifunctional smart optical fibers: materials, fabrication, and sensing applications," *Photonics*, **6**, 48 (2019).
2. S. Pissadakis, "Lab-in-a-fiber sensors: a review," *Microelectron. Eng.* **217**, 111105 (2019).
3. R. Min et al., "Optical fiber sensing for marine environment and marine structural health monitoring: a review," *Opt. Laser Technol.* **140**, 107082 (2021).
4. M. F. Bado and J. R. Casas, "A review of recent distributed optical fiber sensors applications for civil engineering structural health monitoring," *Sensors* **21**(5), 1818 (2021).
5. Y.-N. Zhang et al., "Optical fiber sensors for measurement of heavy metal ion concentration: a review," *Measurement* **158**, 107742 (2020).
6. Y. Zheng et al., "Review of fiber optic sensors in geotechnical health monitoring," *Opt. Fiber Technol.* **54**, 102127 (2020).
7. T. He et al., "Review on optical fiber sensors for hazardous-gas monitoring in mines and tunnels," *IEEE Trans. Instrum. Meas.* **72**, 7003722 (2023).
8. W. Zhu et al., "Enhanced sensitivity of heterocore structure surface plasmon resonance sensors based on local microstructures," *Opt. Eng.* **57**(7), 076105 (2018).
9. Z. Shi et al., "Applications of online UV-Vis spectrophotometer for drinking water quality monitoring and process control: a review," *Sensors* **22**(8), 2987 (2022).
10. K. B. Beć, J. Grabska, and C. W. Huck, "Near-infrared spectroscopy in bio-applications," *Molecules* **25**(12), 2948 (2020).
11. T. Chen et al., "Rapid identification of soil cadmium pollution risk at regional scale based on visible and near-infrared spectroscopy," *Environ. Pollut.* **206**, 217–226 (2015).
12. L. M. Labine and M. J. Simpson, "The use of nuclear magnetic resonance (NMR) and mass spectrometry (MS)-based metabolomics in environmental exposure assessment," *Curr. Opin. Environ. Sci. Health* **15**, 7–15 (2020).
13. A. J. Simpson, M. J. Simpson, and R. Soong, "Nuclear magnetic resonance spectroscopy and its key role in environmental research," *Environ. Sci. Technol.* **46**, 11488–11496 (2012).
14. D. Pawar and S. N. Kale, "A review on nanomaterial-modified optical fiber sensors for gases, vapors and ions," *Microchim. Acta* **186**, 253 (2019).
15. J. Li et al., "Structure design and application of hollow core microstructured optical fiber gas sensor: a review," *Opt. Laser Technol.* **135**, 106658 (2021).
16. A. Pathak and C. Viphavakit, "A review on all-optical fiber-based VOC sensors: heading towards the development of promising technology," *Sens. Actuators A: Phys.* **338**, 113455 (2022)
17. Y. Yang et al., "Optical fiber sensor based on a cholesteric liquid crystal film for mixed VOC sensing," *Opt. Express* **28**(21), 31872–31881 (2020).
18. J. Wu et al., "Lab on optical fiber: surface nano-functionalization for real-time monitoring of VOC adsorption/desorption in metal-organic frameworks," *Nanophotonics* **10**(10), 2705–2716 (2021).
19. M. R. Sardar, M. Faisal, and K. Ahmed, "Design and characterization of rectangular slotted porous core photonic crystal fiber for sensing CO_2 gas," *Sens. Bio-Sens. Res.* **30**, 100379 (2020).
20. K.-J. Kim et al., "Centimeter-scale pillared-layer metal–organic framework thin films mediated by hydroxy double salt intermediates for CO_2 sensor applications," *ACS Appl. Mater. Interfaces* **13**(1), 2062–2071 (2020).
21. A. A. Silva et al., "Hollow-core negative curvature fibers for application in optical gas sensors," *Opt. Eng.* **58**(7), 072011 (2019).
22. M. Sangeetha and D. Madhan, "Ultra sensitive molybdenum disulfide (MoS_2)/graphene based hybrid sensor for the detection of NO_2 and formaldehyde gases by fiber optic clad modified method," *Opt. Laser Technol.* **127**, 106193 (2020).
23. H.-Y. Wen et al., "Advanced NO sensors on notched long-period fiber gratings covered by mesoporous WO_3," *IEEE Sens. J.* **20**(9), 4595–4601 (2020).
24. A. K. C. Theoderaj, D. J. Inbaraj, and C. Mangalaraj, "CdS coated clad-modified fiber optic sensor for detection of NO_2 gas," *Mater. Res. Express* **6**(10), 1050c8 (2019).
25. Y. Zhang et al., "Optical H_2S and SO_2 sensor based on chemical conversion and partition differential optical absorption spectroscopy," *Spectrochim. Acta Part A: Mol. Biomol. Spectrosc.* **210**, 120–125 (2019).
26. E. C. Britto, S. M. Nizar, and P. Krishnan, "A highly sensitive photonic crystal fiber gas sensor for the detection of sulfur dioxide," *Silicon* **14**(18), 12665–12674 (2022).

27. L. Wang et al., "Optical sulfur dioxide sensor based on broadband absorption spectroscopy in the wavelength range of 198–222 nm," *Sens. Actuators B: Chem.* **241**, 146–150 (2017).
28. A. Abbaszadeh, S. Makouei, and S. Meshgini, "Ammonia gas detection using photonic crystal fiber with elliptical holes," *Opt. Eng.* **60**(7), 077105 (2021).
29. R. Bharadwaj et al., "Evanescent wave absorbance based fiber optic biosensor for label-free detection of *E. coli* at 280 nm wavelength," *Biosens. Bioelectron.* **26**(7), 3367–3370 (2011).
30. B. Hales, L. Burgess, and S. Emerson, "An absorbance-based fiber-optic sensor for CO_2 (aq) measurement in porewaters of sea floor sediments," *Mar. Chem.* **59**(1-2), 51–62 (1997).
31. J. Jing et al., "Performance improvement approaches for optical fiber SPR sensors and their sensing applications," *Photonics Res.* **10**(1), 126–147 (2022).
32. Y. Yanase et al., "Development of an optical fiber SPR sensor for living cell activation," *Biosens. Bioelectron.* **25**(5), 1244–1247 (2010).
33. Y. Zhao, Q.-L. Wu, and Y.-N. Zhang, "Simultaneous measurement of salinity, temperature and pressure in seawater using optical fiber SPR sensor," *Measurement* **148**, 106792 (2019).
34. J. Li and M. Zhang, "Physics and applications of Raman distributed optical fiber sensing," *Light: Sci. Appl.* **11**(1), 128 (2022).
35. I. Laarossi, M. Á. Quintela-Incera, and J. M. López-Higuera, "Comparative experimental study of a high-temperature Raman-based distributed optical fiber sensor with different special fibers," *Sensors* **19**(3), 574 (2019).
36. J. M. Ottaway et al., "Spatial heterodyne Raman spectrometer (SHRS) for in situ chemical sensing using sapphire and silica optical fiber Raman probes," *Appl. Spectrosc.* **73**(10), 1160–1171 (2019).
37. M. Zhou, J. Guo, and C. Yang, "Ratiometric fluorescence sensor for Fe^{3+} ions detection based on quantum dot-doped hydrogel optical fiber," *Sens. Actuators B: Chem.* **264**, 52–58 (2018).
38. T. Liu et al., "Smartphone-based hand-held optical fiber fluorescence sensor for on-site pH detection," *IEEE Sens. J.* **19**(20), 9441–9446 (2019).
39. T. Liu et al., "Liquid-core hydrogel optical fiber fluorescence probes," *ACS Sens.* **7**(11), 3298–3307 (2022).
40. K. Wang et al., "Advances in optical fiber sensors based on multimode interference (MMI): a review," *IEEE Sens. J.* **21**(1), 132–142 (2020).
41. J. R. Guzmán-Sepúlveda, R. Guzmán-Cabrera, and A. A. Castillo-Guzmán, "Optical sensing using fiber-optic multimode interference devices: a review of nonconventional sensing schemes," *Sensors* **21**(5), 1862 (2021).
42. Z. Liu et al., "Ultra-sensitive optical fiber sensor based on intermodal interference and temperature calibration for trace detection of copper (II) ions," *Opt. Express* **29**(15), 22992–23005 (2021).
43. C. Cascone et al., "AbspectroscoPY, a Python toolbox for absorbance-based sensor data in water quality monitoring," *Environ. Sci.: Water Res. Technol.* **8**(4), 836–848 (2022).
44. S. F. Memon et al., "A review of optical fibre ethanol sensors: current state and future prospects," *Sensors* **22**(3), 950 (2022).
45. M. M. Alkhabet et al., "Room temperature operated hydrogen sensor using palladium coated on tapered optical fiber," *Mater. Sci. Eng.: B* **287**, 116092 (2023).
46. M. Li et al., "A dual-mode optical fiber sensor for SERS and fluorescence detection in liquid," *Spectrochim. Acta Part A: Mol. Biomol. Spectrosc.* **290**, 122267 (2023).
47. T. Liu et al., "Quantitative remote and on-site Hg^{2+} detection using the handheld smartphone based optical fiber fluorescence sensor (SOFFS)," *Sens. Actuators B: Chem.* **301**, 127168 (2019).
48. M. Yan et al., "Reflective epoxy resin/chitosan/PAA composite-functionalized fiber-optic interferometric probe sensor for sensitive heavy metal ion detection," *Analyst* **148**(5), 1075–1084 (2023).
49. Y. Zhou et al., "Biochemical sensor based on functional material assisted optical fiber surface plasmon resonance: a review," *Measurement* **207**, 112353 (2022).
50. W. Zheng et al., "Highly-sensitive and reflective glucose sensor based on optical fiber surface plasmon resonance," *Microchem. J.* **157**, 105010 (2020).
51. X. Li et al., "Plug-in optical fiber SPR biosensor for lung cancer gene detection with temperature and pH compensation," *Sens. Actuators B: Chem.* **359**, 131596 (2022).
52. L. Li et al., "Optical fiber SPR biosensor based on gold nanoparticle amplification for DNA hybridization detection," *Talanta* **247**, 123599 (2022).
53. Y. Zhao et al., "Current status of optical fiber biosensor based on surface plasmon resonance," *Biosens. Bioelectron.* **142**, 111505 (2019).
54. P. Singh, "SPR biosensors: historical perspectives and current challenges," *Sens. Actuators B: Chem.* **229**, 110–130 (2016).
55. Q. Wang et al., "Research advances on surface plasmon resonance biosensors," *Nanoscale* **14**(3), 564–591 (2022).
56. W. Zhang, J. Ma, and D.-W. Sun, "Raman spectroscopic techniques for detecting structure and quality of frozen foods: principles and applications," *Crit. Rev. Food Sci. Nutr.* **61**(16), 2623–2639 (2021).

57. D. Cialla-May et al., "Raman spectroscopy and imaging in bioanalytics," *Anal. Chem.* **94**(1), 86–119 (2021).
58. F. Zhou et al., "Au-nanorod-clusters patterned optical fiber SERS probes fabricated by laser-induced evaporation self-assembly method," *Opt. Express* **28**(5), 6648–6662 (2020).
59. N. T. T. Phuong et al., "Functionalized silver nanoparticles for SERS amplification with enhanced reproducibility and for ultrasensitive optical fiber sensing in environmental and biochemical assays," *RSC Adv.* **12**(48), 31352–31362 (2022).
60. Y. Long et al., "Hybrid structure design, preparation of Ag-GO SERS optical fiber probe and its chemical, electromagnetic enhancement mechanism," *J. Alloys Comp.* **901**, 163660 (2022).
61. A. I. Pérez-Jiménez et al., "Surface-enhanced Raman spectroscopy: benefits, trade-offs and future developments," *Chem. Sci.* **11**(18), 4563–4577 (2020).
62. A. Tariq et al., "Fluorescent molecular probe based optical fiber sensor dedicated to pH measurement of concrete," *Sens. Actuators B: Chem.* **327**, 128906 (2021).
63. T. Van Tam et al., "Novel paper-and fiber optic-based fluorescent sensor for glucose detection using aniline-functionalized graphene quantum dots," *Sens. Actuators B: Chem.* **329**, 129250 (2021)
64. A. Miliou, "In-fiber interferometric-based sensors: overview and recent advances," *Photonics* **8**, 265 (2021).
65. B. Su et al., "Hybrid fiber interferometer sensor for simultaneous measurement of strain and temperature with refractive index insensitivity," *Opt. Commun.* **522**, 128637 (2022)
66. Y. Zhao et al., "Review of optical fiber Mach–Zehnder interferometers with micro-cavity fabricated by femtosecond laser and sensing applications," *Opt. Laser Eng.* **117**, 7–20 (2019).
67. D. Ming et al., "Trace copper detection using in-line optical fiber Mach–Zehnder interferometer combined with an optoelectronic oscillator," *Opt. Express* **29**(15), 23430–23438 (2021).
68. M. Alonso-Murias et al., "Hybrid optical fiber Fabry–Perot interferometer for nano-displacement sensing," *Opt. Laser Technol.* **155**, 108426 (2022).
69. X. Zhou et al., "A compact hydrogen sensor based on the fiber-optic Fabry–Perot interferometer," *Opt. Laser Technol.* **124**, 105995 (2020).
70. H. Sun et al., "Large core-offset based in-fiber Michelson interferometer for humidity sensing," *Opt. Fiber Technol.* **55**, 102153 (2020).
71. Z. Li et al., "Parallelized fiber Michelson interferometers with advanced curvature sensitivity plus abated temperature crosstalk," *Opt. Lett.* **45**(18), 4996–4999 (2020).
72. W. Lin et al., "Temperature sensor based on fiber ring laser with cascaded fiber optic Sagnac interferometers," *IEEE Photonics J.* **13**(2), 1–12 (2021).
73. W. Zhang et al., "Highly sensitive temperature and strain sensor based on fiber Sagnac interferometer with Vernier effect," *Opt. Commun.* **506**, 127543 (2022).
74. B. S. Boruah and R. Biswas, "Localized surface plasmon resonance based U-shaped optical fiber probe for the detection of Pb^{2+} in aqueous medium," *Sens. Actuators B: Chem.* **276**, 89–94 (2018).
75. S. Triantafyllidou and M. Edwards, "Lead (Pb) in tap water and in blood: implications for lead exposure in the United States," *Crit. Rev. Environ. Sci. Technol.* **42**(13), 1297–1352 (2012).
76. D. B. Akers et al., "Lead (Pb) contamination of self-supply groundwater systems in coastal Madagascar and predictions of blood lead levels in exposed children," *Environ. Sci. Technol.* **49**(5), 2685–2693 (2015).
77. H. R. Ali et al., "Levels of lead (Pb), cadmium (Cd) and cobalt (Co) in cow milk from selected areas of Zanzibar Island, Tanzania," *Am. J. Anal. Chem.* **14**(7), 287–304 (2023).
78. S. Ghosh et al., "Lead (Pb^{2+}) ion sensor development using optical fiber gratings and nanocomposite materials," *Sens. Actuators B: Chem.* **364**, 131818 (2022).
79. S. H. K. Yap et al., "An advanced hand-held microfiber-based sensor for ultrasensitive lead ion detection," *ACS Sens.* **3**(12), 2506–2512 (2018).
80. A. M. Shrivastav and B. D. Gupta, "Ion-imprinted nanoparticles for the concurrent estimation of Pb (II) and Cu (II) ions over a two channel surface plasmon resonance-based fiber optic platform," *J. Biomed. Opt.* **23**(1), 017001 (2018).
81. F. Suhailin et al., "Fiber-based surface plasmon resonance sensor for lead ion detection in aqueous solution," *Plasmonics* **15**, 1369–1376 (2020).
82. M. Nazari et al., "Highly-efficient sulfonated UiO-66 (Zr) optical fiber for rapid detection of trace levels of Pb^{2+}," *Int. J. Mol. Sci.* **22**(11), 6053 (2021).
83. N. Choudhury et al., "Rhodamine-appended polymeric probe: an efficient colorimetric and fluorometric sensing platform for Hg^{2+} in aqueous medium and living cells," *ACS Appl. Polym. Mater.* **2**(11), 5077–5085 (2020).
84. H. M. Gonçalves, A. J. Duarte, and J. C. E. da Silva, "Optical fiber sensor for Hg (II) based on carbon dots," *Biosens. Bioelectron.* **26**(4), 1302–1306 (2010).
85. B. Ninwong et al., "Sensitive distance-based paper-based quantification of mercury ions using carbon nanodots and heating-based preconcentration," *RSC Adv.* **10**(17), 9884–9893 (2020).

86. H. Yuan et al., "Thymine-functionalized gold nanoparticles (Au NPs) for a highly sensitive fiber-optic surface plasmon resonance mercury ion nanosensor," *Nanomaterials* **11**(2), 397 (2021).
87. S. Kraithong et al., "A method to detect Hg^{2+} in vegetable via a "Turn-ON" Hg^{2+}–Fluorescent sensor with a nanomolar sensitivity," *J. Photochem. Photobiol. A: Chem.* **389**, 112224 (2020).
88. M. Lu et al., "Dithiol self-assembled monolayer based electrochemical surface plasmon resonance optical fiber sensor for selective heavy metal ions detection," *J. Lightwave Technol.* **39**(12), 4034–4040 (2021).
89. H. Yuan et al., "Mercaptopyridine-functionalized gold nanoparticles for fiber-optic surface plasmon resonance Hg^{2+} sensing," *ACS Sens.* **4**(3), 704–710 (2019).
90. A.-S. Abedi et al., "A systematic review and meta-analysis of lead and cadmium concentrations in cow milk in Iran and human health risk assessment," *Environ. Sci. Pollut. Res.* **27**, 10147–10159 (2020).
91. S. Cai et al., "Selective detection of cadmium ions using plasmonic optical fiber gratings functionalized with bacteria," *Opt. Express* **28**(13), 19740–19749 (2020).
92. B. Li et al., "Twist-assisted high sensitivity chiral fiber sensor for Cd^{2+} concentration detection," *iScience* **25**(10), 105245 (2022).
93. C. Levantesi et al., "Salmonella in surface and drinking water: occurrence and water-mediated transmission," *Food Res. Int.* **45**(2), 587–602 (2012).
94. R. G. Price and D. Wildeboer, "*E. coli* as an indicator of contamination and health risk in environmental waters," in *Escherichia coli-Recent Advances on Physiology, Pathogenesis and Biotechnological Applications*, p. 3 (2017).
95. S. T. Odonkor and J. K. Ampofo, "*Escherichia coli* as an indicator of bacteriological quality of water: an overview," *Microbiol. Res.* **4**(1), e2 (2013).
96. S. Kaushik et al., "Rapid detection of *Escherichia coli* using fiber optic surface plasmon resonance immunosensor based on biofunctionalized molybdenum disulfide (MoS_2) nanosheets," *Biosens. Bioelectron.* **126**, 501–509 (2019).
97. F. Long et al., "Portable and automated fluorescence microarray biosensing platform for on-site parallel detection and early-warning of multiple pollutants," *Talanta* **210**, 120650 (2020).
98. S. Kaushik et al., "Label-free detection of *Escherichia coli* bacteria by cascaded chirped long period gratings immunosensor," *Rev. Sci. Instrum.* **90**(2), 025003 (2019).
99. P. Halkare et al., "Label-free detection of *Escherichia coli* from mixed bacterial cultures using bacteriophage T4 on plasmonic fiber-optic sensor," *ACS Sens.* **6**(7), 2720–2727 (2021).
100. R. Yang et al., "Development of novel portable and reusable fiber optical chemiluminescent biosensor and its application for sensitive detection of microcystin-LR," *Biosens. Bioelectron.* **121**, 27–33 (2018).
101. Y. Duan et al., "TFBG-SPR DNA-biosensor for renewable ultra-trace detection of mercury ions," *J. Lightwave Technol.* **39**(12), 3903–3910 (2021).
102. K. Sadani, P. Nag, and S. Mukherji, "LSPR based optical fiber sensor with chitosan capped gold nanoparticles on BSA for trace detection of Hg (II) in water, soil and food samples," *Biosens. Bioelectron.* **134**, 90–96 (2019).
103. B. Kavitha et al., "Highly sensitive and rapid detection of mercury in water using functionalized etched fiber Bragg grating sensors," *Sens. Actuators B: Chem.* **333**, 129550 (2021).
104. A. Zhang et al., "Trace detection of cadmium (II) ions based on an air-hole-assisted multicore microstructured optical fiber," *Sens. Actuators B: Chem.* **365**, 131941 (2022).
105. B. S. Boruah, R. Biswas, and U. Baishya, "Ultrasensitive trace determination of cadmium through a green synthesized hybrid PVA-chitosan nanocomposite," *Plasmonics* **15**, 1903–1912 (2020).
106. M. Singh and S. K. Raghuwanshi, "Real-time interrogation of fiber optic biosensor using TiO_2 coated etched long-period grating," *Rev. Sci. Instrum.* **91**(12), 125001 (2020).
107. A. K. Mandal et al., "Detection of microcystin-LR in water using polyaniline coated U-bent fiber optic biosensor," in *IEEE Appl. Sens. Conf. (APSCON)*, IEEE, pp. 1–3 (2023).
108. A. Afzal et al., "NO_x sensors based on semiconducting metal oxide nanostructures: progress and perspectives," *Sens. Actuators B: Chem.* **171**, 25–42 (2012).
109. C. Di Franco et al., "Optical and electronic NO_x sensors for applications in mechatronics," *Sensors* **9**(5), 3337–3356 (2009).
110. K. Xu et al., "A room temperature all-optical sensor based on two-dimensional SnS_2 for highly sensitive and reversible NO_2 sensing," *J. Hazard. Mater.* **426**, 127813 (2022).
111. X. Bian et al., "Continuous measurement of NO_2 in flue gas employing cavity-enhanced spectroscopy sensing system," *Measurement* **201**, 111729 (2022).
112. J. Zou and F. Wang, "Simultaneous measurement of SO_2 and NO_2 concentration using an optical fiber-based LP-DOAS system," *Chin. Opt. Lett.* **18**(2), 021201 (2020).
113. B. Peng et al., "An ultra-sensitive detection system for sulfur dioxide and nitric oxide based on improved differential optical absorption spectroscopy method," *Spectrochim. Acta Part A: Mol. Biomol. Spectrosc.* **233**, 118169 (2020).

114. J. Mohanraj et al., "All fiber-optic multigas (NH_3, NO_2, and CO) sensor based on $MoWS_2$ coated fiber," *IEEE Sens. J.* **22**(13), 12869–12876 (2022).
115. Q. Yao et al., "2D plasmonic tungsten oxide enabled ultrasensitive fiber optics gas sensor," *Adv. Opt. Mater.* **7**(24), 1901383 (2019).
116. S. J. Mechery and J. P. Singh, "Fiber optic based gas sensor with nanoporous structure for the selective detection of NO_2 in air samples," *Anal. Chim. Acta* **557**(1–2), 123–129 (2006).
117. W. Wu et al., "A real-time and highly sensitive fiber optic biosensor based on the carbon quantum dots for nitric oxide detection," *J. Photochem. Photobiol. A: Chem.* **405**, 112963 (2021).
118. Y. Niu et al., "MoS_2 graphene fiber based gas sensing devices," *Carbon* **95**, 34–41 (2015).
119. M. Majder-Łopatka et al., "The influence of hydrogen on the indications of the electrochemical carbon monoxide sensors," *Sustainability* **12**(1), 14 (2019).
120. S. Mahajan and S. Jagtap, "Metal-oxide semiconductors for carbon monoxide (CO) gas sensing: a review," *Appl. Mater. Today* **18**, 100483 (2020).
121. J. Peng et al., "Fiber-optic dual Fabry–Pérot interferometric carbon monoxide sensor with polyaniline/Co_3O_4/graphene oxide sensing membrane," *Chin. Chem. Lett.* **31**(8), 2145–2149 (2020).
122. J. Zhou, X. Huang, and W. Feng, "Carbon monoxide gas sensor based on Co/Ni-MOF-74 coated no-core-fiber Michelson interferometer," *Physica Scr.* **98**(1), 015012 (2022).
123. S. He et al., "Carbon monoxide gas sensor based on an α-Fe_2O_3/reduced graphene oxide quantum dots composite film integrated Michelson interferometer," *Meas. Sci. Technol.* **33**(3), 035102 (2021).
124. C. Chen and W. Feng, "Intensity-modulated carbon monoxide gas sensor based on cerium dioxide-coated thin-core-fiber Mach–Zehnder interferometer," *Opt. Laser Technol.* **152**, 108183 (2022).
125. C. Yao et al., "Photothermal CO detection in a hollow-core negative curvature fiber," *Opt. Lett.* **44**(16), 4048–4051 (2019).
126. Z. Liu, L. Zhu, and G. Yan, "Fast gas sensing scheme with multi-component gas measurement capacity based on non-dispersive frequency comb spectroscopy (ND-FCS)," *Opt. Express* **31**(5), 8785–8796 (2023).
127. M. R. Miah et al., "Polypyrrole-based sensors for volatile organic compounds (VOCs) sensing and capturing: a comprehensive review," *Sens. Actuators A: Phys.* **347**, 113933 (2022).
128. H. Lin, M. Jang, and K. S. Suslick, "Preoxidation for colorimetric sensor array detection of VOCs," *J. Am. Chem. Soc.* **133**(42), 16786–16789 (2011).
129. C. Elosua et al., "Volatile organic compound optical fiber sensors: a review," *Sensors* **6**(11), 1440–1465 (2006).
130. J. Wang et al., "Tailor-made photonic crystal fiber sensor for the selective detection of formaldehyde and benzene," *Opt. Fiber Technol.* **52**, 101941 (2019).
131. L. Dong et al., "A vapochromic dye/graphene coated long-period fiber grating for benzene vapor sensing," *Mater. Chem. Front.* **6**(17), 2438–2446 (2022).
132. D. Pawar et al., "High-performance dual cavity-interferometric volatile gas sensor utilizing graphene/PMMA nanocomposite," *Sens. Actuators B: Chem.* **312**, 127921 (2020).
133. G. D. Bhise et al., "Optical fibre based acetone sensor using Pd modified WO_3 nanostructures," *Opt. Laser Technol.* **156**, 108566 (2022).
134. C. Yao et al., "Sub-ppm CO detection in a sub-meter-long hollow-core negative curvature fiber using absorption spectroscopy at 2.3 μm," *Sens. Actuators B: Chem.* **303**, 127238 (2020).
135. B. Renganathan et al., "High proficient sensing response in clad modified ceria doped tin oxide fiber optic toxic gas sensor application," *Sens. Actuators A: Phys.* **332**, 113114 (2021).
136. M. Rivai, T. A. Sardjono, and D. Purwanto, "Investigation of Michelson interferometer for volatile organic compound sensor," *J. Phys.: Conf. Ser.* **853**, 012017 (2017).
137. R. Kanawade et al., "Negative axicon tip-based fiber optic interferometer cavity sensor for volatile gas sensing," *Opt. Express* **27**(5), 7277–7290 (2019).
138. Y. Li et al., "A self-assembled fiber Mach–Zehnder interferometer based on liquid crystals," *J. Mater. Chem. C* **8**(32), 11153–11159 (2020).
139. J. Hromadka et al., "Highly sensitive volatile organic compounds vapour measurements using a long period grating optical fibre sensor coated with metal organic framework ZIF-8," *Sens. Actuators B: Chem.* **260**, 685–692 (2018).

Dajuan Lyu received her MSc degree in materials science and engineering from Wuhan University of Technology in 2011, respectively, where she is currently pursuing her PhD at the National Engineering Research Center for Fiber Optic Sensing Technology and Networks. Her research interests include optical fiber materials, fiber-optic sensors, and fiber Bragg gratings.

Qing Huang received her PhD in materials science and engineering from Wuhan University of Technology in 2021. She is currently working as a postdoctoral at the School of Integrated

Circuits of Huazhong University of Science and Technology. Her research interests include optical fiber surface plasmon resonance technology and biochemical sensing.

Xiaokun Wu received his bachelor's degree in marine technology from Wuhan University of Technology in 2013. He is currently working as an engineer at Wuchang Shipbuilding Heavy Industry Group Co., Ltd., China. His research interest includes oceanic water quality monitoring.

Yanbo Nie received his bachelor's degree in materials science and engineering from Wuhan University of Technology in 2023. He is currently pursuing his PhD at the School of Materials Science and Engineering of Wuhan University of Technology. His research interest includes optical fiber sensing.

Minghong Yang received his PhD in physics from Huazhong University of Science and Technology, China, in 2003. He is currently a research scientist at the National Engineering Research Center for Fiber Optic Sensing Technology and Networks, Wuhan University of Technology, China. His research interests include thin-film optical fiber sensors.